The Astrophysical Journal Supplement Series, 178:225–246, 2008 October

MOLECULAR GAS DISTRIBUTION IN BARRED AND NONBARRED GALAXIES ALONG THE HUBBLE SEQUENCE

S. Komugi,[1,2,3] Y. Sofue,[1,4] K. Kohno,[1] H. Nakanishi,[4,5] S. Onodera,[1] F. Egusa,[1,3] and K. Muraoka[1,3]

Received 2008 January 9; accepted 2008 May 26

ABSTRACT

We present results from a survey of ^{12}CO ($J = 1$–0) spectra obtained for the central regions of 68 nearby galaxies at an angular resolution of 16″ using the Nobeyama Radio Observatory 45 m telescope, aimed at characterizing the properties of star-forming molecular gas. Combined with observations of similar resolution in the literature, the compiled sample set of 166 galaxies span a wide range of galactic properties. NGC 4380, which was previously undetected in CO, was detected. This initial paper of a series will focus on the data and the gaseous properties of the samples, and particularly on the degree of central concentration of molecular gas in a range of morphological types, from early (S0/Sa) to late (Sd/Sm) galaxies with and without bars. The degree of molecular central concentration in the central kiloparsec, compared with the central several kiloparsecs of galaxies, is found to vary smoothly with Hubble type, so that early-type galaxies show larger central concentration. The comparison of barred and nonbarred galaxies within early- and late-type galaxies suggest that difference in Hubble type, representing the effect of bulges, is the more important factor in concentrating gas into the central regions than bars.

Subject headings: galaxies: spiral — ISM: molecules

Online material: color figures

1. INTRODUCTION

Molecular gas is the driving element of star formation in galaxies, and its quantitative relation to the current star formation rate is essential to our understanding of galactic evolution. It has become increasingly clear that the dynamical properties of galaxies are responsible for redistributing molecular gas on large scales, and hence the star formation that follows, is also affected by the dynamical properties. These dynamical properties are expressed as large-scale features (morphology) of the galaxies, i.e., the presence bars and difference between Hubble type. These two features (presence of bars and Hubble type) are most prominent and characteristic in the central kiloparsecs of galaxies, which is also where most of the molecular gas in galaxies is present. Therefore, the distribution of gas within the central region of various morphologies and its relation with star formation has gained attention in recent years.

Bars on kpc scales at the centers of galaxies are known to redistribute angular momentum and transfer molecular gas to the centers. Sakamoto et al. (1999b) showed that molecular gas in barred galaxies has a higher degree of concentration in its central 1 kpc compared with gas inside the optical disk, by using interferometric data from the Nobeyama Millimeter Array (NMA) and Owens Valley Radio Observatory (OVRO) at 4″ resolution. Similarly, Sheth et al. (2005) showed by using the Berkeley-Illinois-Maryland-Array (BIMA) at 6″ resolution that the central 1 kpc of barred galaxies has 4 times more molecular gas compared with the global average. Some barred galaxies in their sample were not detected, and they attribute it to the quenching of gas due to efficient star formation in barred galaxies. Single-dish observations have also proved effective. By using the Nobeyama Radio Observatory[6] (NRO) 45 m telescope, Kuno et al. (2007) mapped out 40 nearby galaxies at 16″ resolution. They defined the "inner" central concentration $f_{\rm in}$ as the ratio between molecular mass in 1/8 of the K-band radius (defined at 20 mag arcsec^{-1} in the K_S band) and that within one-half of the K-band radius. They similarly defined the "outer" central concentration $f_{\rm out}$ as the ratio between molecular mass in one-half of the K-band radius and that within the whole of the K-band radius. They found that barred galaxies have a significantly higher $f_{\rm in}$, whereas the $f_{\rm out}$ did not show much dependence. Furthermore, they found a correlation between $f_{\rm in}$ and the bar strength.

It seems that molecular gas concentration due to bars is a well established phenomenon, and this has also been explored in terms of numerical simulations (Combes & Gerin 1985; Pfenniger & Norman 1990; Athanassoula 1992; Wada & Habe 1995).

Molecular gas is also known to be distributed differently between early- and late-type galaxies. Molecular gas mass in the centers of galaxies has been found to decrease in later Hubble types (e.g., Young & Knezek 1989; Böker et al. 2003). This has been attributed to the existence of a stellar bulge in early-type galaxies (Young & Knezek 1989) creating a deep potential well in which gas is accumulated. Even in the absence of stellar bulges, possible correlations with nuclear star clusters and stellar surface brightness have been found (Böker et al. 2003). Sheth et al. (2005) report a fourfold central molecular mass increase in barred early-type galaxies compared with barred late-type galaxies. Early-type galaxies, however, have been found to host stronger bars than late-types, with larger $m = 2$ and $m = 4$ Fourier amplitudes (Laurikainen & Salo 2002; but see also Laurikainen et al. 2004). This points to the possibility that early-type galaxies may show larger central concentration simply because they host stronger bars.

[1] Institute of Astronomy, University of Tokyo, 2–21–1 Osawa, Mitaka-shi, Tokyo, 181–8588, Japan.
[2] National Astronomical Observatory of Japan.
[3] Japan Society for the Promotion of Science for Young Scientists Research Fellowship for Young Scientists.
[4] Kagoshima University, Kagoshima, Japan.
[5] Australia Telescope National Facility/CSIRO, Epping, NSW, Australia.

[6] Nobeyama Radio Observatory is a branch of the National Astronomical Observatory of Japan, National Institutes of Natural Sciences.

TABLE 1
GALAXIES OBSERVED AT THE NRO 45 METER TELESCOPE

Galaxy (1)	R.A. (J2000.0) (2)	Decl. (J2000.0) (3)	Distance (Mpc) (4)
NGC 253	00 47 35.2	−25 17 20	2.2
NGC 520	01 24 34.7	+03 47 49.8	30.3
NGC 772	01 59 20.3	+19 00 22	34.1
NGC 877	02 17 58.7	+14 32 50.3	54.9
NGC 908	02 23 04.8**	−21 14 06	19.6
NGC 1022	02 38 32.9**	−06 40 29	20.1
NGC 1482	03 54 39.4**	−20 30 08.5	20.5
NGC 1569	04 30 50.3	+64 50 48	3.1
NGC 1961	05 42 04.3	+69 22 46	54.1
NGC 2276	07 27 14.4*	+85 45 16	34.4
NGC 2336	07 27 04.1*	+80 10 41	31.9
NGC 2339	07 08 20.5*	+18 46 49	31.1
NGC 2403	07 36 54.5	+65 35 58.4	2.2
NGC 2559	08 17 07.5**	−27 27 34	17.3
NGC 2683	08 52 41.3*	+33 25 19	3.2
NGC 2976	09 47 15.6	+67 54 49	2.3
NGC 3034	09 55 54.0	+69 40 57	2.2
NGC 3147	10 16 53.6*	+73 24 03	38.4
NGC 3556	11 11 30.9	+55 40 27	10.3
NGC 3593	11 14 37.0*	+12 49 04	7.3
NGC 3623	11 18 56.0*	+13 05 32.0	4.5
NGC 3631	11 21 02.9*	+53 10 11	16.6
NGC 3675	11 26 08.6*	+43 35 09	9.8
NGC 3690	11 28 33.6	+58 33 51.3	41.4
NGC 3893	11 48 39.1	+48 42 40	13.8
NGC 3938	11 52 49.8	+44 07 26	11.2
NGC 4038	12 01 53.0**	−18 51 48	19.2
NGC 4039	12 01 54.2**	−18 53 06	19.2
NGC 4041	12 02 12.2*	+62 08 14	17.6
NGC 4088	12 05 35.3	+50 32 31	16.4
NGC 4096	12 06 01.0	+47 28 31	11.2
NGC 4157	12 11 04.4*	+50 29 05	12.1
NGC 4178	12 12 46.4*	+10 51 57	16.1
NGC 4212	12 15 39.3*	+13 54 06	16.1
NGC 4293	12 21 12.9*	+18 22 57	16.1
NGC 4298	12 21 32.8*	+14 36 22	16.1
NGC 4302	12 21 42.4	+14 36 05	16.1
NGC 4321	12 22 54.9*	+15 49 20	16.1
NGC 4380	12 25 22.2*	+10 01 00	16.1
NGC 4394	12 25 55.6*	+18 12 50	16.1
NGC 4418	12 26 54.2	−00 52 45	25.5
NGC 4419	12 26 56.4*	+15 02 51	16.1
NGC 4424	12 27 11.6*	+09 25 14	16.1
NGC 4527	12 34 08.8	+02 39 13	16.1
NGC 4536	12 34 27.1*	+02 11 16	16.1
NGC 4548	12 35 55.2*	+14 29 47	16.1
NGC 4567	12 36 32.7*	+11 15 29	16.1
NGC 4568	12 36 34.7	+11 14 15	16.1
NGC 4647	12 43 32.3*	+11 34 55	16.1
NGC 4666	12 45 08.9	−00 27 38	18.6
NGC 4689	12 47 45.5*	+13 45 46	16.1
NGC 4691	12 48 14.1**	−03 19 51	13.1
NGC 4698	12 48 23.5	+08 29 16	16.1
NGC 4710	12 49 38.9*	+15 09 56	16.1
NGC 4818	12 56 48.7**	−08 31 25	13.5
NGC 4845	12 58 01.4	+01 34 30	16.1
NGC 4984	13 08 57.3**	−15 30 59	14.7
NGC 5236	13 36 59.4	−29 52 04	5.9
NGC 5247	13 38 03.5	−17 53 02	20.1
NGC 5713	14 40 11.5	−00 17 26	24.6
NGC 5861	15 09 16.5**	−11 19 24	24.1
NGC 6000	15 49 49.4	−29 23 13	27.1
NGC 6814	19 42 40.1**	−10 19 27	21.1
NGC 6946	20 34 51.9	+60 09 15	6.7
NGC 6951	20 37 15.2	+66 06 22	21.7
NGC 7479	23 04 57.1	+12 19 18	34.7
NGC 7541	23 14 43.0	+04 32 05	38.1
IC 342	03 46 49.7	+68 05 45	3.0

NOTES.—Col. (1): Galaxy name. Cols. (2) and (3): Right ascension and declination (J2000.0), from Dressel & Condon (1976) unless otherwise noted. Units of right ascension are hours, minutes, and seconds, and units of declination are degrees, arcminutes, and arcseconds. Coordinates with one asterisk are from NED, coordinates with two asterisks are from RC2. All of the coordinates of the different references were found to be consistent within the beam size of the FCRAO survey, 45″, and mostly within 6″, except for NGC 1022, NGC 2559, and NGC 4038. Col. (4): Distance as listed in Young et al. (1995) scaled using Hubble constant $H_0 = 75$ km s^{-1} Mpc^{-1}. NGC 4874 from Liu & Graham (2001). For members of the Virgo cluster, 16.1 Mpc is assumed from Cepheid calibrations (Ferrarese et al. 1996).

It is important, therefore, to quantify which factor (the presence of bars or Hubble type) plays the larger role in redistributing gas to the central regions of galaxies.

Mapping observations in CO are optimum for the study of molecular gas distribution in nearby galaxies, but available galaxy samples are limited by the vast observing time needed for such projects (e.g., Sakamoto et al. 1999a; Helfer et al. 2003; Sofue et al. 2003). In turn, single-beam measurements at the centers of a large sample of galaxies lack the precision in terms of spatial distribution of molecular gas but can compensate for the lack of number of sample galaxies. In this respect, quantifying the CO content of nearby galactic centers for a large sample using single-dish telescopes is still rewarding.

In order to complement existing studies on molecular gas concentration in galaxies of various morphology, we have conducted a large survey of the central region of nearby galaxies using NRO 45 m telescope. Our data provide a unique opportunity to study the gas distribution in the central region, with several advantages: (1) samples are distributed mostly at the distance of 16 Mpc, and therefore the single beam subtends a similar scale of the central 1 kpc of galaxies; (2) many of our samples are also observed by Young et al. (1995) using the FCRAO 14 m dish, with an angular resolution of 45″ or a linear scale of 3 kpc. Therefore, the ratio of CO intensity measured by the different surveys can be interpreted as a degree of central concentration of molecular gas.

2. SAMPLE SELECTION

The sample galaxies have been selected from those observed and detected in the FCRAO catalog (Young et al. 1995; Kenney & Young 1988) of nearby galaxies. The FCRAO survey is the largest CO survey of nearby galaxies (300 galaxies), spanning a wide range of parameter space for spirals, but with a large beam size of 45″. All of our observing samples, mainly spirals, come from galaxies observed in this survey. Since one of the secondary aims of our survey is compare the CO data with star formation (to be presented in forthcoming papers), galaxies in the FCRAO survey were selected on whether they had available Hα data as listed in Young et al. (1996) and also with measured Hα/Hβ ratios (to be used to correct for internal dust extinction) in Ho et al. (1997). Ninety-one galaxies meet these criteria, of which 14 were already observed at either the NRO 45 m or the IRAM 30 m telescope, which has a similar beam size as the

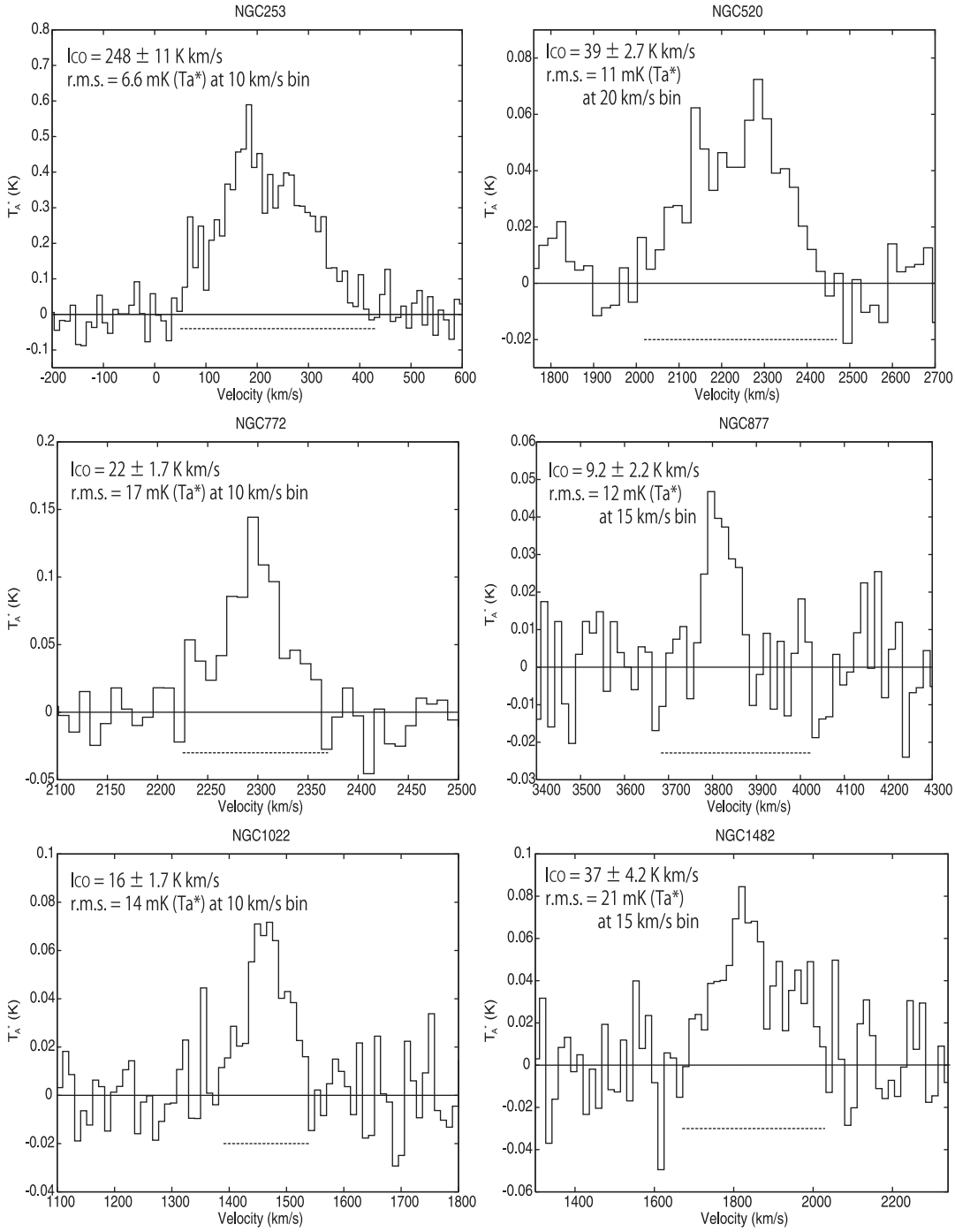

FIG. 1.— Spectra of the galaxies observed at NRO 45 m telescope, with S/N over 5. Abscissa is the heliocentric velocity. Emission is indicated by the dotted horizontal line, selected with reference to Young et al. (1995) or Kenney & Young (1988).

NRO 45 m telescope. Therefore, the final selected sample consisted of 77 galaxies. Galaxies in the FCRAO survey were selected to span a wide variety of galaxies and were not magnitude or volume limited. Our sample also follows this idea.

In the observation (see § 3), 38 of the 77 were actually observed, due mainly to weather conditions. An additional five, with Hα data from Young et al. (1996) but without Hα/Hβ, and 25 with observations from the FCRAO survey but not Hα, were observed. These galaxies without Hα measurements were simply selected by whether they were observable at that certain period. Thus, our observed sample consists of 68 galaxies. Table 1 lists the observed samples.

3. OBSERVATIONS

The observations of the ^{12}CO ($J = 1$–0) line (rest frequency 115.27 GHz) were conducted with the 45 m telescope at the Nobeyama Radio Observatory (NRO) of the National Astronomical Observatory of Japan, during three observing runs in 2005 May, 2005 December, and 2006 January, under moderate weather conditions. Two superconductor-insulator-superconductor (SIS) receivers, S100 and/or S80, were used for the observations. The back ends were the 1024 channel digital autocorrelator with a frequency coverage of 512 MHz, or the 2048 channel acousto-optical spectrometer with a frequency coverage of 250 MHz. The

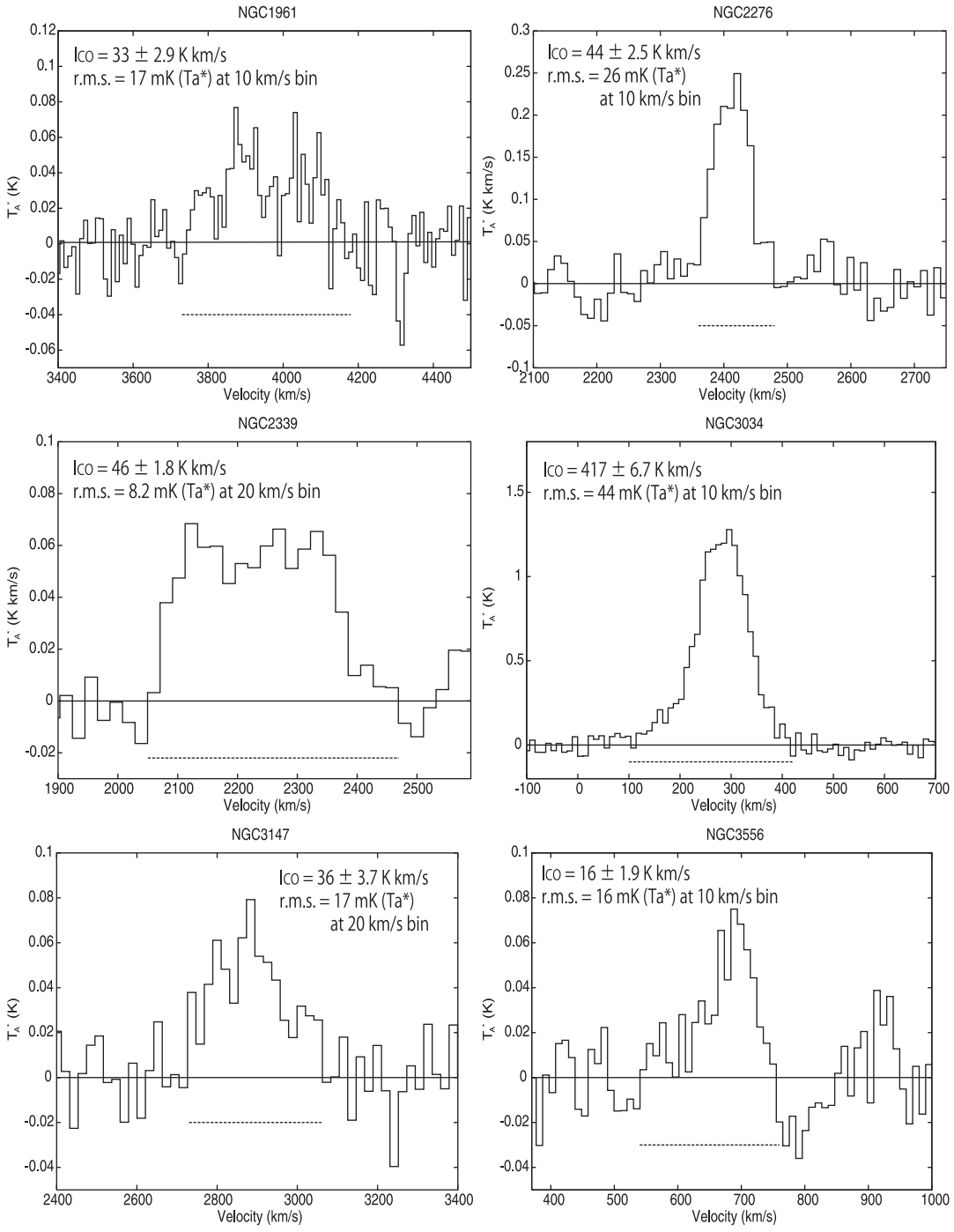

FIG. 1—*Continued*

CO line was observed in the upper sideband. Typical system temperatures ranged from 700 to 2000 K in the 2005 May run, and from 450 to 1000 K (all in single-sideband scale) in the 2005 December and 2006 January run. The beam width was 16″. Pointing was checked using SiO masers or continuum sources at 43 GHz every 0.5–1 hr and found to be accurate within 5″ unless otherwise noted where wind prevented pointing at such accuracy. Each of the target galaxies was observed with a single beam at the center.

The obtained data were reduced with the NEWSTAR software used commonly at NRO, which is based on the Astronomical Image Processing System (AIPS) package, developed by the National Radio Astronomy Observatory. After flagging bad spectra, first- or second-order baselines were subtracted, and then the antenna temperature T_A^* was converted to main beam temperature $T_{\rm mb}$ through $T_{\rm mb} = T_A^*/\eta_{\rm mb}$, where $\eta_{\rm mb}$ is the main beam efficiency, taken to be 0.38 based on 2004 November observations of the Saturn and 3C 279. The typical rms noise ranged from 10 to 20 mK, after reduction. The spectra were then binned into velocities that best showed the emission features (typically 10 km s^{-1} or 15 km s^{-1}). The integrated intensity $I_{\rm CO}$ is calculated by $I_{\rm CO} = \int T_{\rm mb}\, dv$, where the range of velocity for integration was chosen with reference to spectra from the FCRAO catalog (Young et al. 1995 or Kenney &

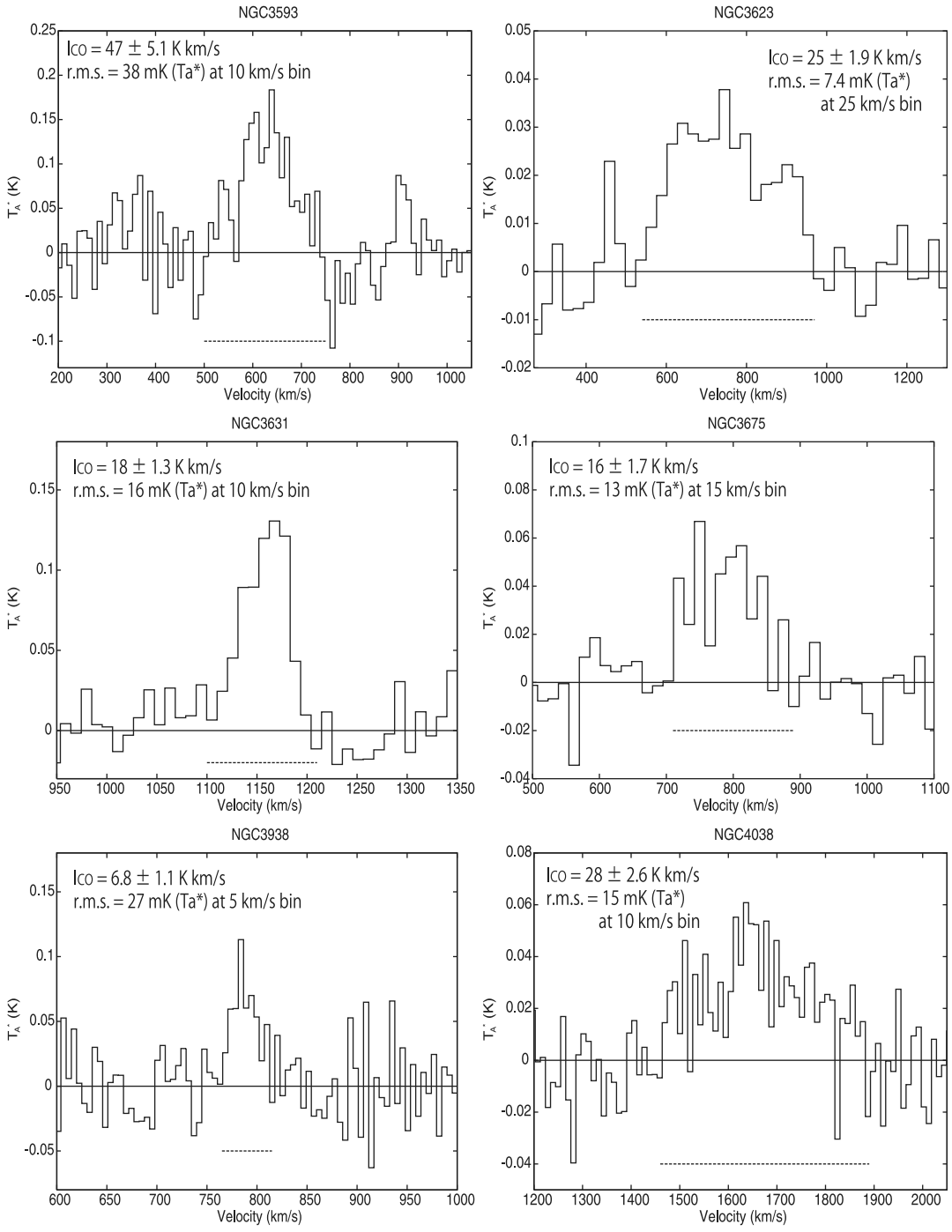

FIG. 1—*Continued*

Young 1988). The errors for the line intensities were calculated as

$$\delta I_{\rm CO} = \sigma\sqrt{\Delta V_{\rm CO}\delta V} \quad [\rm K\ km\ s^{-1}], \tag{1}$$

where σ is the rms noise in $T_{\rm mb}$, $\Delta V_{\rm CO}$ the full line width, and δV is the velocity resolution (5, 10, 15, or 20 km s^{-1}).

For spectra with signal-to-noise ratio of less than 3, the upper limits were calculated by

$$I_{\rm CO} \leq 3\sigma\sqrt{\Delta V_{\rm CO}\delta V} \quad [\rm K\ km\ s^{-1}]. \tag{2}$$

For those galaxies that were detected in the FCRAO survey but not ours, the same $\Delta V_{\rm CO}$ was assumed. For galaxies that were detected in neither sample, an arbitrary $\Delta V_{\rm CO}$ of 100 km s^{-1} was assumed.

The observational errors presented in the following section are only for the rms errors of the baseline. In general, other sources of error (pointing error, baseline subtraction, and calibration) that are difficult to quantify are dominant sources of error for millimeter observations. Three galaxies (NGC 6951, NGC 6946, and IC 342) were observed both in this study and the survey by Nishiyama & Nakai (2001) at the same telescope. The integrated intensities of NGC 6951 and IC 342 are consistent to within

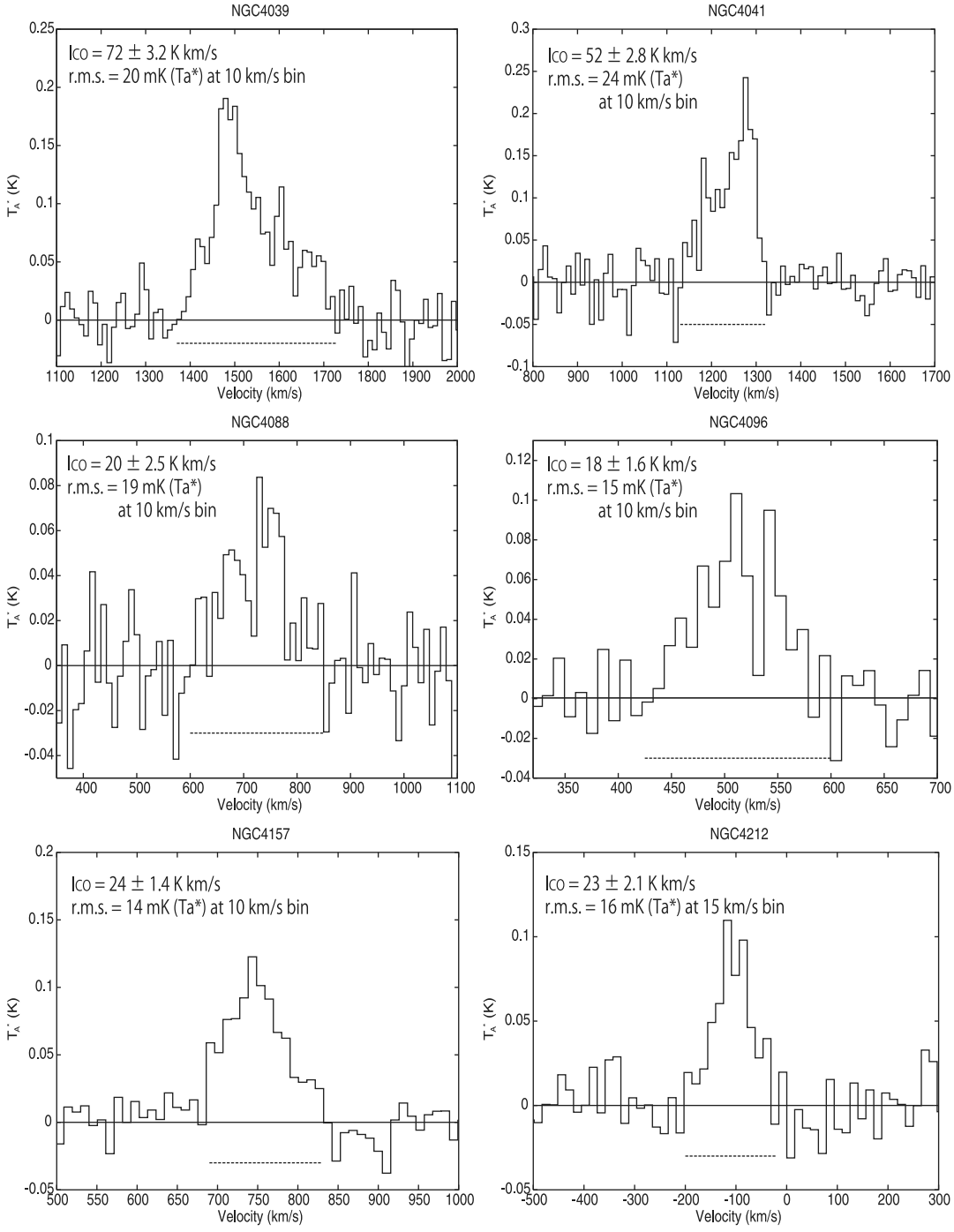

FIG. 1—*Continued*

30%. For NGC 6946, Nishiyama & Nakai (2001) give a value that is ~50% of this study but may be attributed to the bad observing condition in our study (system temperature 1400 K). For most of the samples, therefore, readers should assume a typical error of ~30% for the obtained integrated intensities.

4. RESULTS

We show the spectra of the observed galaxies in Figure 1 (detected galaxies followed by tentative detections and non-detections). Of the 68 galaxies observed, 54 were detected at a signal-to-noise ratio (S/N) of more than 5, and 60 galaxies with S/N more than 3 (see Fig. 2). All analysis in this paper will be limited toward galaxies with S/N over 5.

5. OTHER DATA AND CONSISTENCY

In addition to the data gathered in this study at the NRO 45 m telescope, other galaxies that were observed in other previous studies either at NRO 45 m or the IRAM 30 m telescope were compiled. The IRAM 30 m telescope has a beam width of 22″, similar to the NRO 45 m telescope. After compilation, we have a total sample of 166 galaxies observed in CO at the central region. Furthermore, 117 of these were observed by Young et al. (1995)

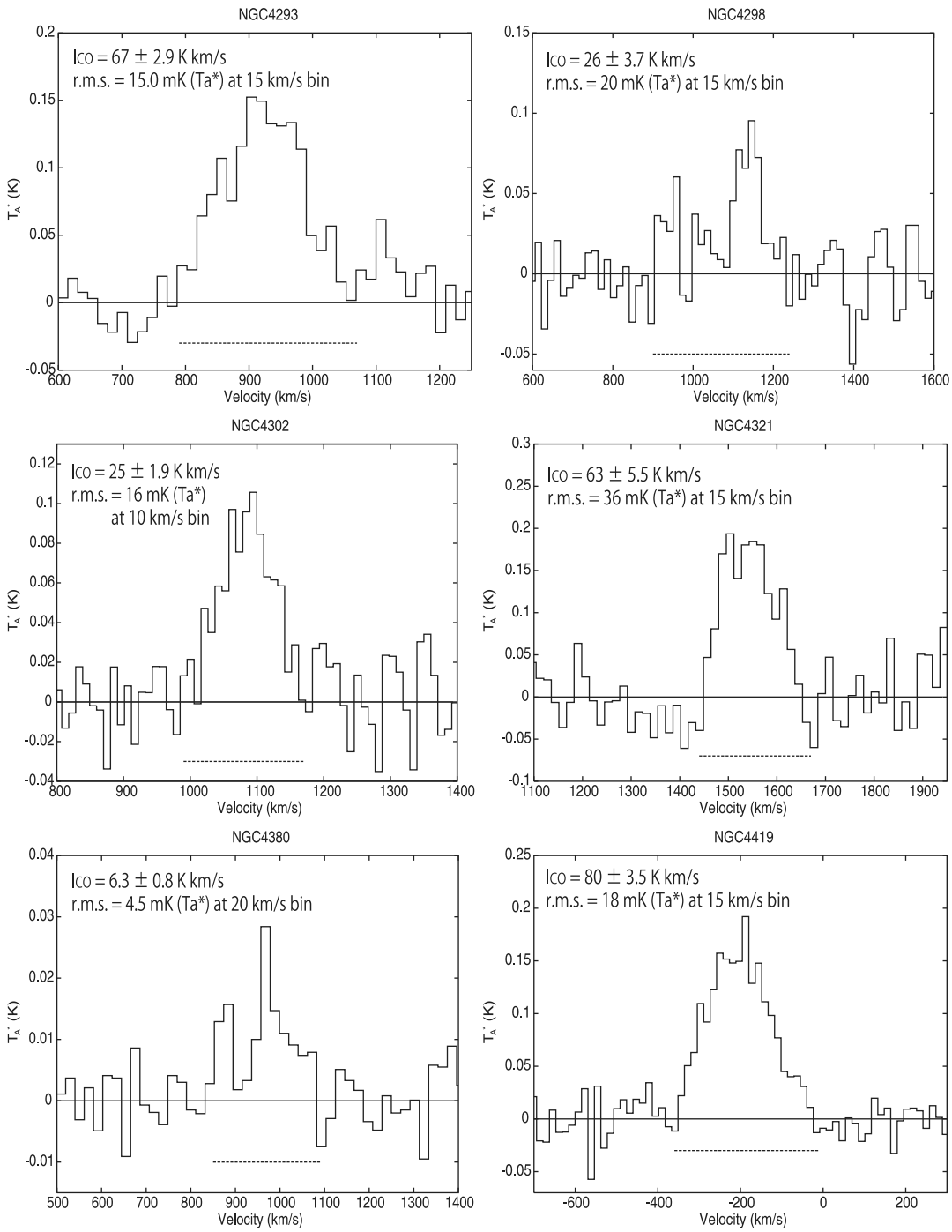

FIG. 1—*Continued*

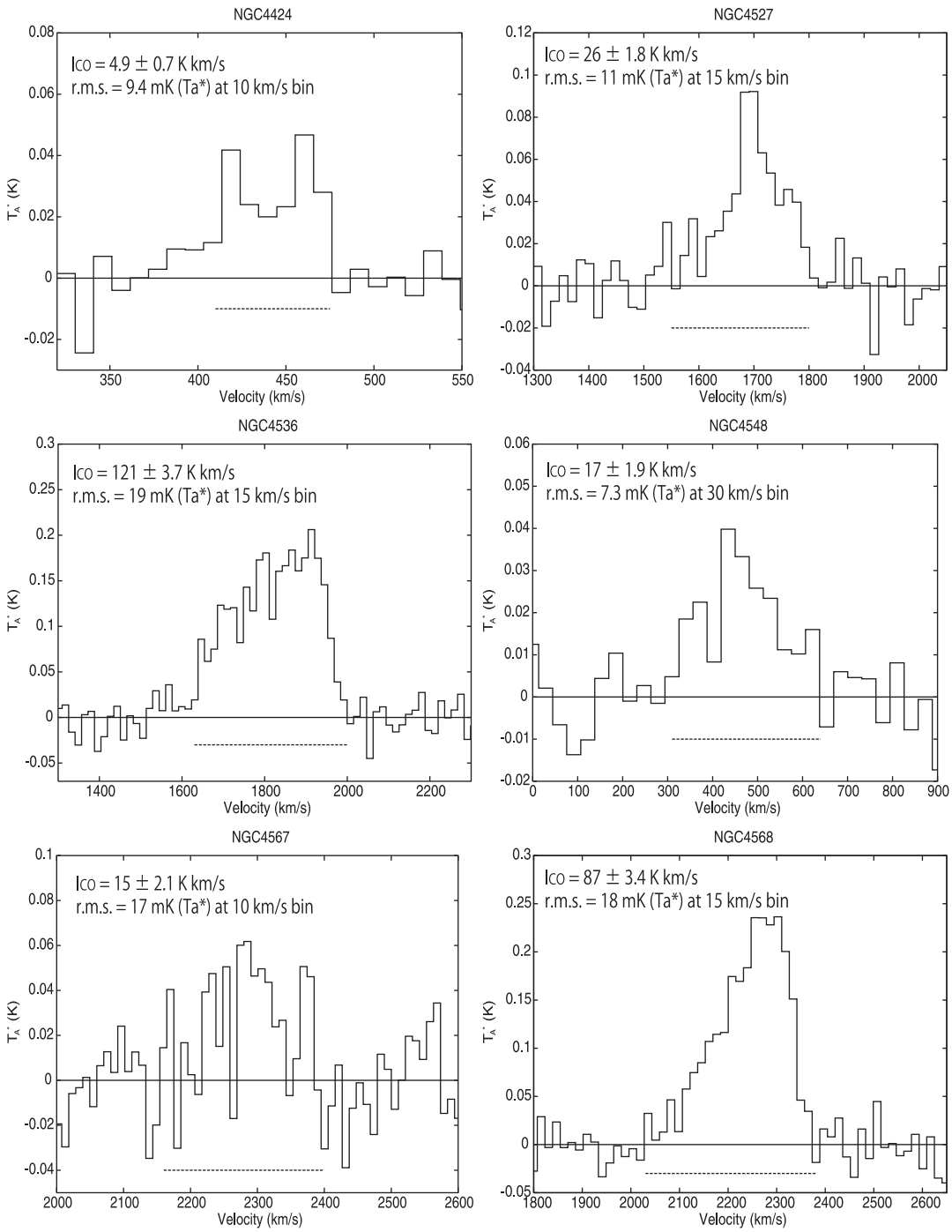

FIG. 1—*Continued*

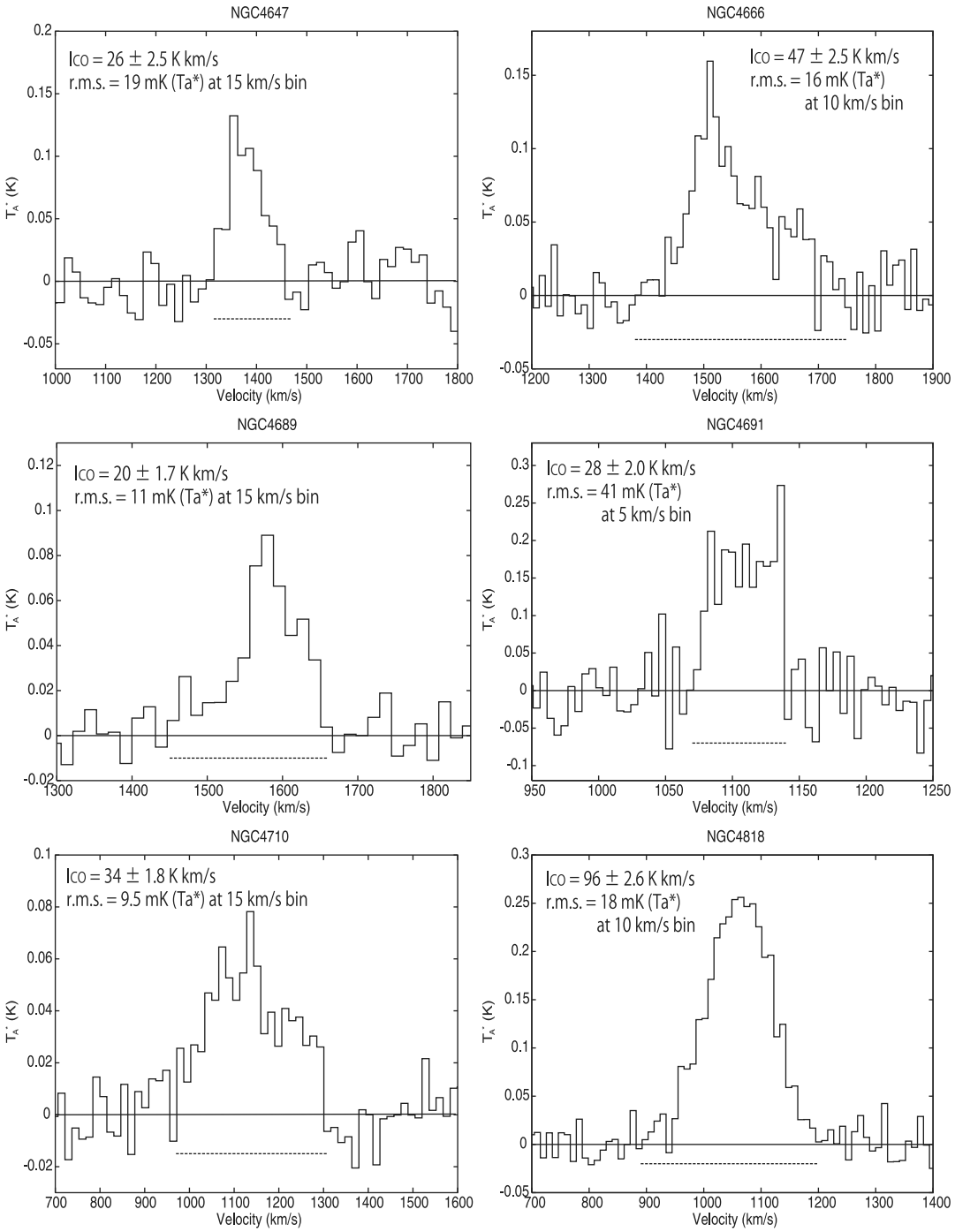

FIG. 1—*Continued*

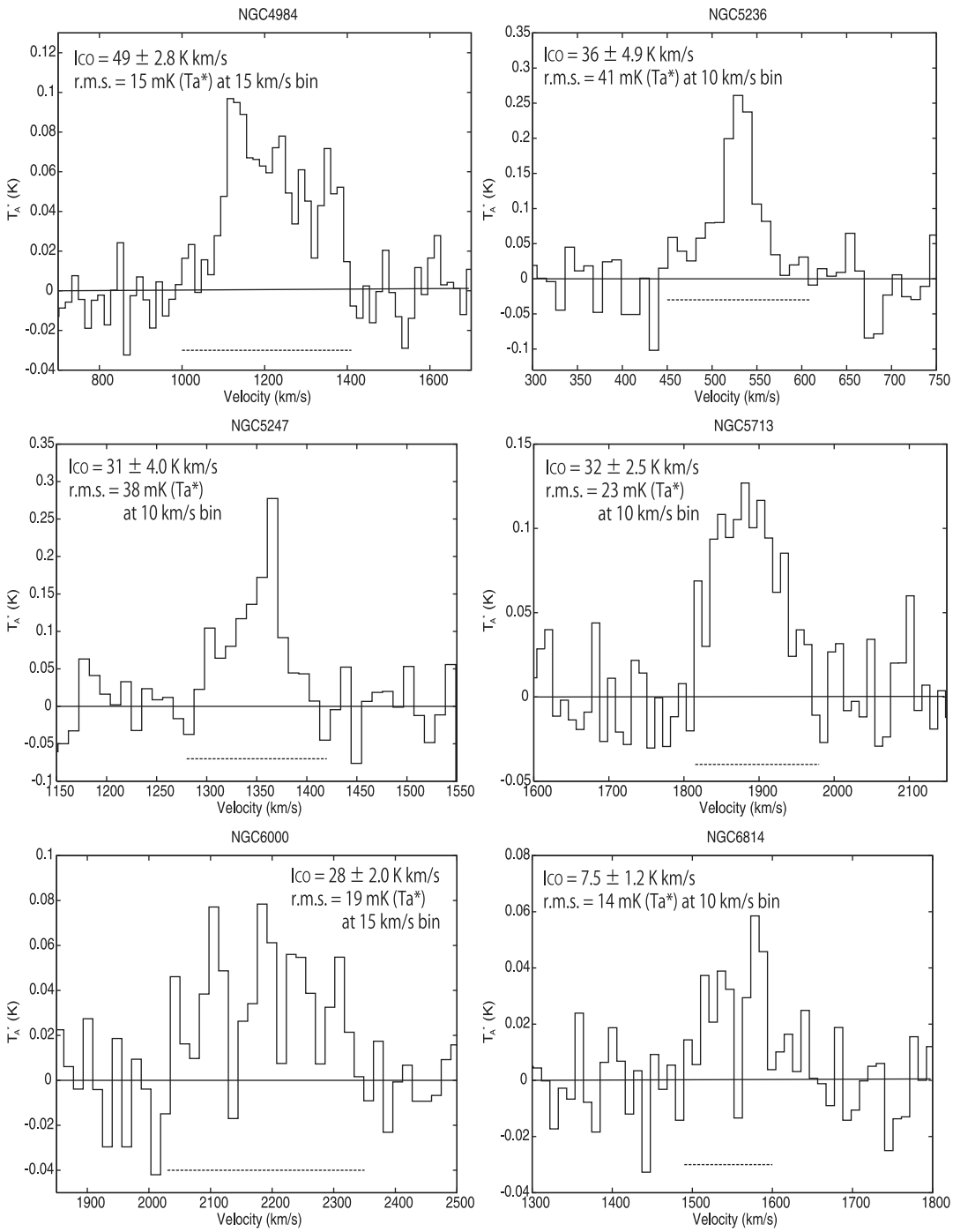

FIG. 1—*Continued*

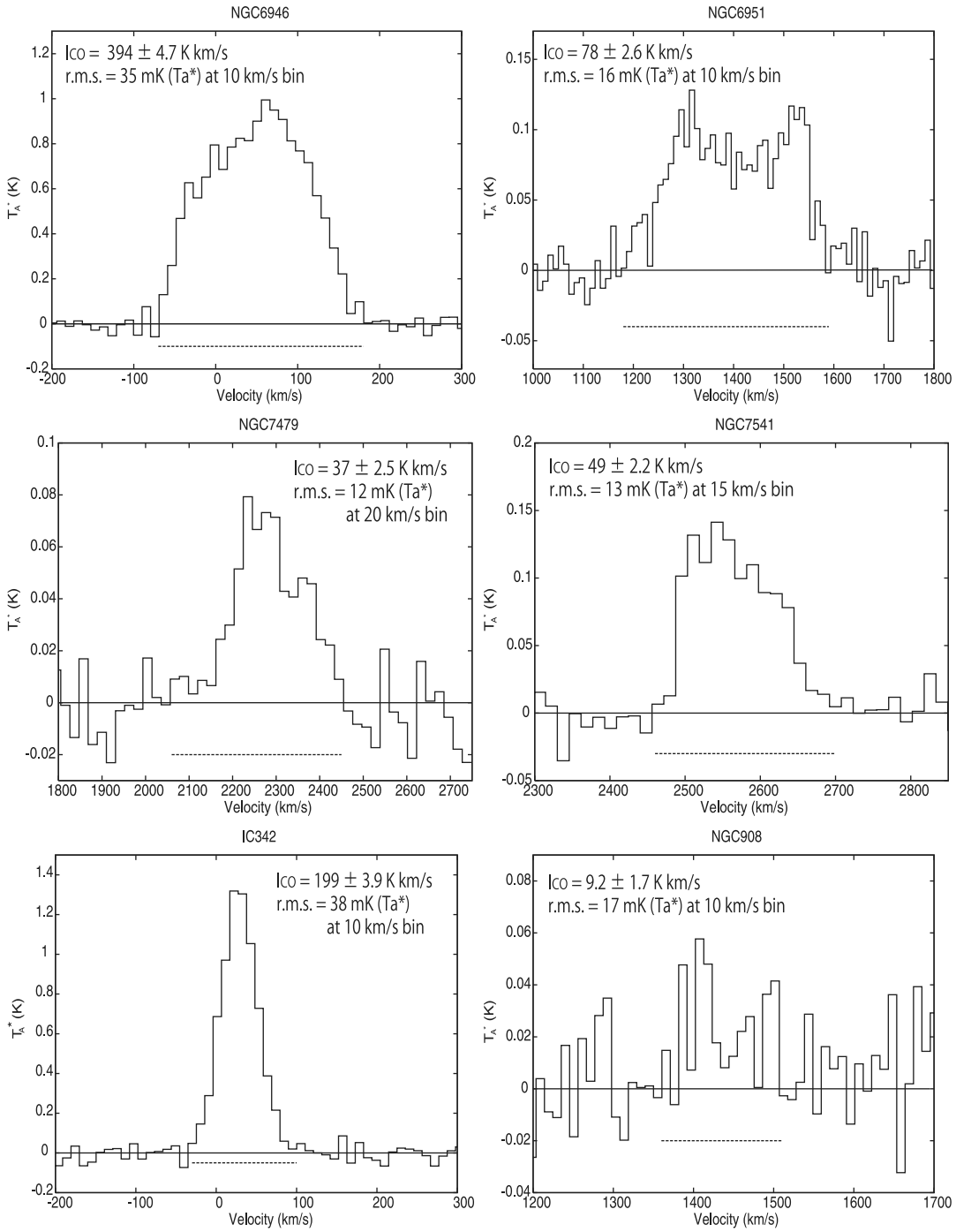

FIG. 1—*Continued*

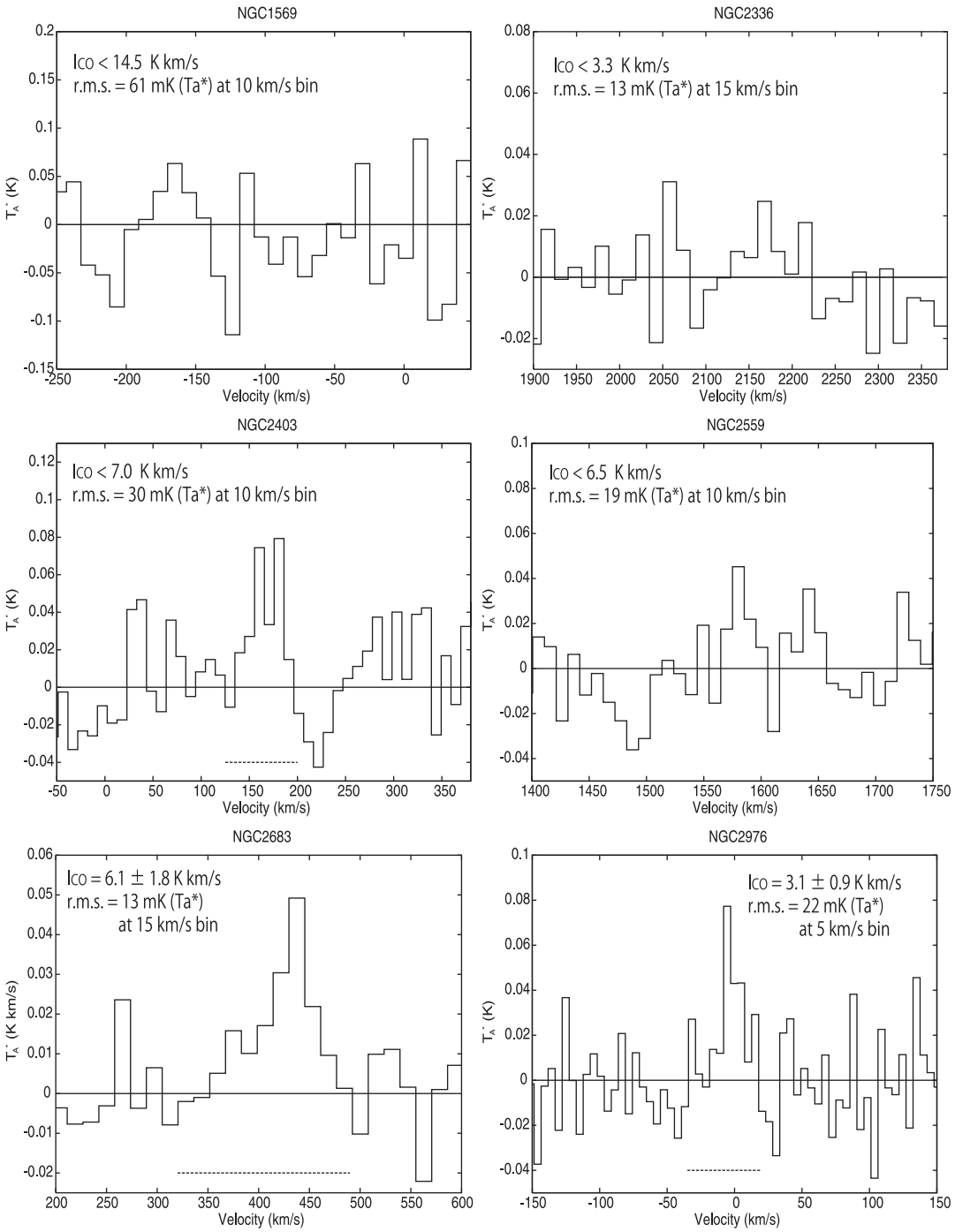

FIG. 2.—Same as Fig. 1, for galaxies below S/N of 5. Integrated intensity is shown only for those over S/N of 3, and upper limits for S/N less than 3.

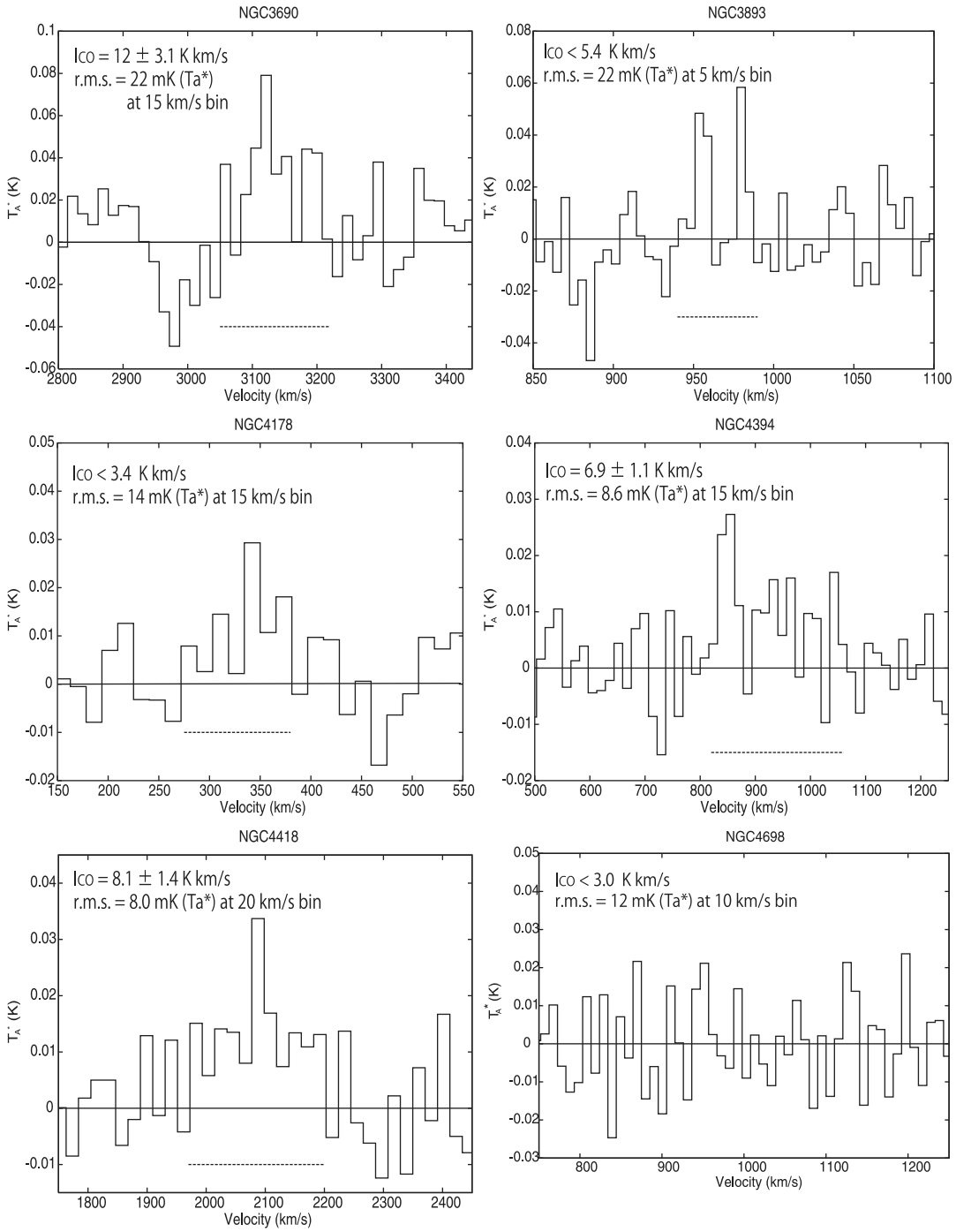

FIG. 2—*Continued*

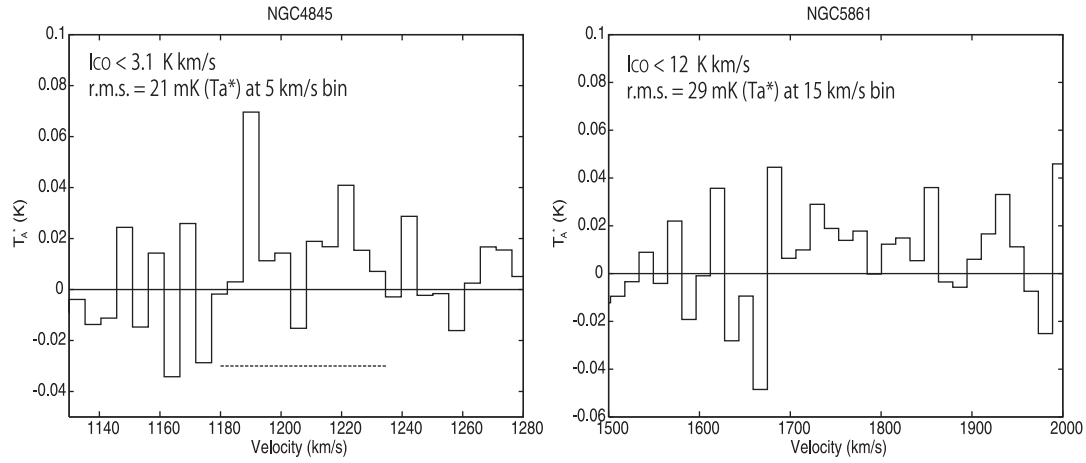

FIG. 2—*Continued*

or Kenney & Young (1988) with 45″ resolution. Table 2 lists the compiled data, along with the derived integrated intensities from this study.

Although the beam width of the IRAM 30 m telescope at 22″ is similar to that of the NRO 45 m telescope at 16″, it is important that CO detected at both telescopes can be compared on a same scale. In order to confirm this point, Figure 3 plots the derived integrated intensity I_{CO} for galaxies that overlapped between observations at NRO 45 m and IRAM 30 m telescope. A clear proportionality with a slope of order unity can be seen, despite the small number of samples. The zero point of this relation is effectively 0, despite the difference in beam size, enabling a direct comparison of observed intensity.

Three galaxies deviate from the relation in Figure 3 by more than a factor of 2 (NGC 3810, NGC 5033, and NGC 7331). All of these galaxies are from Nishiyama & Nakai (2001) and Braine et al. (1993) for the NRO 45 m and IRAM 30 m measurements, respectively. NGC 3810 has a starbursting nucleus, and its I_{CO} at a single beam away from its nucleus drops to nearly half the value found by Nishiyama & Nakai (2001). The observing coordinates in Nishiyama & Nakai (2001) and Braine et al. (1993) are offset by 4″, possibly explaining the excess of I_{CO} in the NRO 45 m measurement. The I_{CO} for NGC 5033 also drops by more than 50% 11″ from the center in Nishiyama & Nakai (2001), making the CO intensity consistent with that of Braine et al. (1993). The offset in observing coordinates (∼2″) coupled with pointing errors may account for the discrepancy. The observing coordinates for NGC 7331 differ by 14″. Since the coordinates in Braine et al. (1993) are offset from the true center, the difference in I_{CO} may reflect the central CO hole, which explains the smaller CO intensity in Nishiyama & Nakai (2001). Nevertheless, it is important to bear in mind that when comparing CO intensities from the different telescopes, an error of typically a factor of 2 may in fact be involved.

A secondary check can be implemented by using the 45″ resolution data from the FCRAO data of Young et al. (1995). The ratio of CO intensity at NRO 45 m or IRAM 30 m telescope to the FCRAO intensity expresses a measure of the central condensation of gas; if the angular resolution difference of the NRO 45 m and IRAM 30 m telescope has a significant effect on the derived intensity, this ratio should display a systematic difference between the two telescopes. Figure 4 plots the CO intensity observed at the FCRAO I_{CO}^{FC} versus the intensity observed either at the NRO 45 m or IRAM 30 m telescope, including those only with more than a 3 σ detection. A clear correlation can be seen, and a least-squares fit to the CO intensity from the NRO 45 m telescope I_{CO}^{NRO} gives

$$\log I_{CO}^{NRO} = (0.91 \pm 0.14) \log I_{CO}^{FC} + (0.78 \pm 0.14), \quad (3)$$

whereas the same fit to the IRAM 30 m telescope will give

$$\log I_{CO}^{IRAM} = (0.94 \pm 0.09) \log I_{CO}^{FC} + (0.63 \pm 0.08). \quad (4)$$

Both fits are consistent within the range of error, and we conclude that the data from these two telescopes with different beam sizes can be compared on the same scale without correction.

6. SAMPLE PROPERTIES

Figure 5 shows the distance distribution of our compiled samples from the NRO 45 m and IRAM 30 m dishes. The samples are strongly peaked at around 16 Mpc, where the Virgo cluster members lie. The distances here are taken from Young et al. (1995) scaled to $H_0 = 75$ km s^{-1} Mpc^{-1} except for Virgo cluster members, where a more recent measurement (Ferrarese et al. 1996) gives 16.1 Mpc using Cepheid variables. The observing beam of 16″ and 22″ for 16 Mpc correspond to a linear scale of 1.2 and 1.8 kpc, respectively. These both correspond to radii within 1 kpc of the center, and considering that most of our samples lie around this distance, we will simply refer hereafter to these data as gas in the "central kpc" and its corresponding CO intensity I_{CO}^{NRO} or I_{CO}^{IRAM} as $I_{1\,kpc}$. CO measured in Young et al. (1995) and Kenney & Young (1988) with the 45″ beam size will be referred to as gas in the "central 3 kpc," denoted $I_{3\,kpc}$. The reader should refer to Table 2 for the actual linear scale of the measurement for individual galaxies.

Figure 6 shows the distribution of morphology for all sample galaxies detected in CO at the central kpc. The Hubble types are taken from the HyperLEDA database (Paturel et al. 2003). Most galaxies lie on Hubble type 4–5, corresponding to Sbc–Sc on de Vaucouleur's scale. No apparent biases are seen in regard to the fraction of barred/nonbarred galaxies in certain Hubble types, although we have significantly fewer SB galaxies compared with SA or SAB galaxies in total. A weak bias may exist that more barred galaxies are observed in the latest types, but this may also be representative of the general galaxy population (e.g., Abraham & Merrifield 2000).

The inclination (i) of the target galaxies result in a variation in the projected area of the observing beam. This is especially important in our case because we observed the galaxies with only

TABLE 2

COMPILED GALAXY SAMPLES

Galaxy (1)	I_{CO} (K km s^{-1}) (2)	Reference (3)	Distance (Mpc) (4)	I_{CO}^{FC} (K km s^{-1}) (5)	Hubble Type (HyperLEDA) (6)	Morphology (NED) (7)
NGC 157	23 ± 0.9	2	23.3	9.02	4.0	SAB(rs)bc
NGC 253	248 ± 11	1	2.2	467	5.1	SAB(s)c
NGC 278	18 ± 0.8	2,6	11.8	14.2	2.9	SAB(rs)b
NGC 337a	<0.46	5	13.3*	35.5	7.9	SAB(s)dm
NGC 520	39 ± 2.7	1	20.2	30.2	0.8	Pec
NGC 628	4.1 ± 0.3	2,6	10.6	4.15	5.2	SA(s)c
NGC 660	99 ± 1.3	2	13.1	38.2	1.3	SB(s)a pec
NGC 772	22 ± 1.7	1	34.1	16.1	3.0	SA(s)b
NGC 864	6 ± 0.9	2	21.8	1.31	5.1	SAB(rs)c
NGC 877	10 ± 1.6	1	54.9	12.9	4.8	SAB(rs)bc
NGC 891	96 ± 5	2	9.4	26.2	3.0	SA(s)b sp
NGC 908	9.2 ± 1.7	1	19.6	18.9	5.1	SA(s)c
NGC 925	1.9 ± 0.5	2	9.5	1.18	7.0	SAB(s)d
NGC 1022	16 ± 1.7	1	20.1	9.67	1.1	SB(s)a
NGC 1042	2.9 ± 0.3	2	19.1**	...	6.0	SAB(rs)cd
NGC 1055	46 ± 1.6	2	14.3	41.1	3.2	SBb sp
NGC 1068	218 ± 7	3	15.1	99.8	3.0	SA(rs)b
NGC 1084	31 ± 2.2	2	18.7	11.5	4.9	SA(s)c
NGC 1087	15 ± 1	2	24.6	6.86	5.2	SAB(rs)c
NGC 1482	37 ± 4.2	1	20.5	20.0	−0.9	SA0+ pec sp
NGC 1569	<14.5	1	3.1	1.82	9.6	IBm
NGC 1637	13 ± 0.7	2	9.5**	...	5.0	SAB(rs)c
NGC 1961	33 ± 2.9	1	54.1	29.5	4.2	SAB(rs)c
NGC 2146	118 ± 1.9	2	13.7	68.4	2.3	SB(s)ab pec
NGC 2276	44 ± 2.5	1	34.4	11.4	4.0	SAB(rs)c
NGC 2336	<3.3	1	31.9	<1.01	5.4	SAB(r)bc
NGC 2339	46 ± 1.8	1	31.1	16.8	4.0	SAB(rs)bc
NGC 2403	<7.0	1	2.2	4.91	6.0	SAB(s)cd
NGC 2559	<6.5	1	17.3	32.1	9.0	SB(s)bc pec
NGC 2681	30 ± 0.8	2	10.1	7.6	3.1	SAB(rs)0/a
NGC 2683	6.1 ± 1.8	1	3.2	5.07	0.4	SA(rs)b
NGC 2715	7.6 ± 1.5	2	20.3**	...	5.2	SAB(rs)c
NGC 2805	2.3 ± 0.1	5	26.2*	...	6.9	SAB(rs)d
NGC 2820	9.8 ± 1.1	2	22.9**	...	5.4	SB(s)c pec sp
NGC 2841	6 ± 0.6	2	9.3	1.46	3.0	SA(r)b
NGC 2903	119 ± 2.3	6	6.2	24	4.0	SB(s)d
NGC 2964	25 ± 0.9	2	16.8	11.4	4.1	SAB(r)bc
NGC 2976	3.1 ± 0.9***	1	2.3	2.07	5.3	SAc pec
NGC 2985	12 ± 2.9	2	19.1	9.55	2.3	SA(rs)ab
NGC 3034	417 ± 6.7	1	2.2	289	8.0	I0
NGC 3079	212 ± 2.7	2	16.1	69.3	6.6	SB(s)c
NGC 3147	36 ± 3.7	1	38.4	10.5	3.9	SA(rs)bc
NGC 3184	7.8 ± 1	6	7.9	5.8	5.0	SAB(rs)cd
NGC 3187	3.5 ± 0.6	2	20.0**	...	5.9	SB(s)c pec
NGC 3198	11 ± 0.5	2	9.3**	...	5.2	SB(rs)c
NGC 3227	54 ± 3.7	2	14.3**	...	1.4	SAB(s) pec
NGC 3310	3.6 ± 0.9	2	14.2	2.15	4.0	SAB(r)bc pec
NGC 3344	4.3 ± 0.4	2	6.9	4.69	4.0	SAB(r)bc
NGC 3346	3.6 ± 0.23	5	17.5*	...	6.0	SB(rs)cd
NGC 3351	17 ± 1.9	2	9.0	14.6	3.0	SB(r)b
NGC 3359	3 ± 1	2	15.0	4.95	5.2	SB(rs)c
NGC 3368	35 ± 1	2	10.3	24.4	1.8	SAB(rs)ab
NGC 3423	2.7 ± 0.24	5	13.6*	...	6.0	SA(s)cd
NGC 3445	0.89 ± 0.1	5	30.0*	...	8.9	SAB(s)m
NGC 3486	7 ± 1	2	9.0	0.76	5.2	SAB(r)c
NGC 3504	103 ± 3.1	6	19.7	13.7	2.1	SAB(s)ab
NGC 3521	17 ± 1.1	6	8.5	22.7	4.0	SAB(rs)bc
NGC 3556	16 ± 1.9	1	10.3	14.4	6.0	SB(s)cd
NGC 3593	47 ± 5.1	1	7.3	18.6	−0.4	SA(s)0/a
NGC 3623	25 ± 1.9	1	4.5	<1.90	1.0	SAB(rs)a
NGC 3627	90 ± 4	2	4.5	34	3.0	SAB(rs)a
NGC 3628	130 ± 5.7	2	4.5	69.5	3.1	SAb pec sp
NGC 3631	18 ± 1.3	1	16.6	7.66	5.2	SA(s)c

TABLE 2—*Continued*

Galaxy (1)	I_{CO} (K km s^{-1}) (2)	Reference (3)	Distance (Mpc) (4)	I_{CO}^{FC} (K km s^{-1}) (5)	Hubble Type (HyperLEDA) (6)	Morphology (NED) (7)
NGC 3675	16 ± 1.7	1	9.8	12.2	3.0	SA(s)b
NGC 3690	12 ± 3.1	1	41.4	19.5	8.7	IBm pec
NGC 3782	0.68 ± 0.11	5	12.6*	...	6.6	SAB(s)cd
NGC 3810	24 ± 2	1,6	11.5	14.3	5.2	SA(rs)c
NGC 3893	<5.4	1	13.8	9.72	5.1	SAB(rs)c
NGC 3906	0.37 ± 0.12	5	15.6*	...	6.8	SB(s)d
NGC 3913	1.9 ± 0.22	5	15.9*	...	6.6	SA(rs)d
NGC 3938	6.8 ± 1.1	1	11.2	8.86	5.1	SA(s)c
NGC 4038	28 ± 2.6	1	19.3	29.3	8.9	SB(s)m pec
NGC 4039	72 ± 3.2	1	19.3	29.6	8.9	SA(s)m pec
NGC 4041	52 ± 2.8	1	17.6	20.4	4.0	SA(rs)bc
NGC 4088	20 ± 2.5	1	10.9	15.6	4.8	SAB(rs)bc
NGC 4096	18 ± 1.6	1	7.5	5.07	5.3	SAB(rs)c
NGC 4102	115 ± 9	6	13.1	17.5	3.0	SAB(s)b
NGC 4157	24 ± 1.4	1	12.1	21.9	3.3	SAB(s)b sp
NGC 4178	<3.4	1	16.1	1.64	7.1	SB(rs)dm
NGC 4204	0.50 ± 0.14	5	12.9*	...	7.9	SB(s)dm
NGC 4212	23 ± 2.1	1	16.1	7.46	4.9	SAc
NGC 4254	47 ± 7.4	6	16.1	19.3	5.2	SA(s)c
NGC 4274	10 ± 0.4	2	11.9**	...	1.7	SB(r)ab
NGC 4293	67 ± 1.1	1	16.1	11.5	0.3	SB(s)0/a
NGC 4298	26 ± 3.7	1	16.1	10.9	5.2	SA(rs)c
NGC 4299	0.48 ± 0.14	5	16.1	1.11	8.3	SAB(s)dm
NGC 4302	25 ± 1.9	1	16.1	8.91	5.4	Sc sp
NGC 4303	69 ± 2.1	6	16.1	21.6	4.0	SAB(rs)bc
NGC 4314	24 ± 0.3	2	10.9**	...	1.0	SB(rs)a
NGC 4321	63 ± 5.5	1,2	16.1	27.3	4.0	SAB(s)bc
NGC 4380	6.3 ± 0.8	1	16.1	<0.1	2.3	SA(rs)b
NGC 4394	6.9 ± 1.1	1	16.1	3.27	8.8	SB(r)b
NGC 4411	0.88 ± 0.10	5	17.8*	...	5.4	SB(rs)c
NGC 4414	79 ± 5.5	2,6	9.6	31.6	5.1	SA(rs)c
NGC 4416	5.08 ± 0.19	5	19.3*	...	5.9	SB(rs)cd
NGC 4418	8.1 ± 1.4	1	25.5	4.91	1.0	SAB(s)a
NGC 4419	80 ± 3.5	1	16.1	18.6	1.1	SB(s)a
NGC 4424	4.9 ± 0.7	1	16.1	1.45	3.0	SB(s)a
NGC 4438	70 ± 7	4	16.1	5.27	0.7	SA(s)0/a pec
NGC 4487	3.23 ± 0.15	5	13.6*	...	5.9	SAB(rs)cd
NGC 4496A	2.17 ± 0.18	5	23.6*	...	7.5	SB(rs)m
NGC 4501	51 ± 2.5	6	16.1	21.8	3.4	SA(rs)b
NGC 4527	26 ± 1.8	1	16.1	28.7	4.0	SAB(s)bc
NGC 4535	42 ± 1.2	6	16.1	8.55	5.0	SAB(s)c
NGC 4536	121 ± 3.7	1	16.1	18.4	4.2	SAB(rs)bc
NGC 4540	5.57 ± 0.19	5	16.1	1.50	6.1	SAB(rs)cd
NGC 4548	17 ± 1.9	1	16.1	6.73	3.1	SBb(rs)
NGC 4565	12 ± 1.2	2	15.7**	...	3.2	SA(s)b sp
NGC 4567	15 ± 2.1	1	16.1	8.55	4.0	SA(rs)bc
NGC 4568	87 ± 3.4	1	16.1	19.1	4.1	SA(rs)bc
NGC 4569	134 ± 3.2	6	16.1	26.6	2.4	SAB(rs)ab
NGC 4618	0.72 ± 0.17	5	10.0*	...	8.6	SB(rs)m
NGC 4625	3.78 ± 0.11	5	10.9*	...	8.8	SAB(rm)m pec
NGC 4647	26 ± 2.5	1	16.1	9.09	5.2	SAB(rs)c
NGC 4651	6 ± 1	2	16.1	7.64	5.2	SA(rs)c
NGC 4654	24 ± 0.9	2	16.1	6.0	5.9	SAB(rs)cd
NGC 4666	47 ± 2.5	1	18.6	30.2	5.0	SABc
NGC 4688	0.44 ± 0.08	5	13.9*	...	6.0	SB(s)cd
NGC 4689	20 ± 1.7	1	16.1	6.55	4.7	SA(rs)bc
NGC 4691	28 ± 2.0	1	13.1	4.8	0.4	SB(s)0/a pec
NGC 4698	<3.0	1	16.1	<0.73	1.4	SA(s)ab
NGC 4701	2.9 ± 0.22	5	10.3*	...	5.8	SA(s)cd
NGC 4710	34 ± 1.8	1	16.1	7.82	−0.8	SA(r)0 sp
NGC 4736	61 ± 3.9	6	4.0	17.5	2.4	SA(r)ab
NGC 4775	1.63 ± 0.22	5	20.9*	...	6.9	SA(s)d
NGC 4818	96 ± 2.6	1	13.5	16.8	2.0	SAB(rs)ab pec
NGC 4826	140 ± 1.9	6	5.0	44.7	2.4	SA(rs)ab

TABLE 2—*Continued*

Galaxy (1)	I_{CO} (K km s^{-1}) (2)	Reference (3)	Distance (Mpc) (4)	I_{CO}^{FC} (K km s^{-1}) (5)	Hubble Type (HyperLEDA) (6)	Morphology (NED) (7)
NGC 4845	<3.1	1	16.1	6.07	2.3	SA(s)ab sp
NGC 4984	49 ± 2.8	1	14.7	12.3	−0.8	SAB(rs)0
NGC 5005	76 ± 5.4	2	14.3	30.4	4.0	SAB(rs)bc
NGC 5033	59 ± 4	2,6	12.8	13.1	5.2	SA(s)c
NGC 5112	1.7 ± 0.4	2	13.4**	...	5.8	SB(rs)cd
NGC 5236	36 ± 4.9	1	5.9	88.7	5.0	SAB(s)c
NGC 5247	31 ± 4	1	20.1	7.67	4.0	SA(s)bc
NGC 5248	67 ± 2.3	6	14.7	19.5	4.1	SB(rs)bc
NGC 5364	5 ± 1	2	18.0	1.00	4.0	SA(rs)bc pec
NGC 5668	1.78 ± 0.26	5	22.2*	...	6.0	SA(s)d
NGC 5669	2.28 ± 0.27	5	19.8*	...	6.9	SAB(rs)cd
NGC 5713	32 ± 2.5	1	24.6	11.0	4.0	SAB(rs)bc pec
NGC 5725	1.12 ± 0.24	5	22.8*	...	7.0	SB(s)d
NGC 5861	<12	1	24.1	10.2	5.0	SAB(rs)c
NGC 5907	32 ± 1.6	2	10.4	7.49	5.4	SA(s)c sp
NGC 5921	6 ± 1.8	2	19.0**	...	4.0	SB(r)bc
NGC 5964	0.89 ± 0.17	5	20.7*	...	6.9	SB(rs)d
NGC 6000	28 ± 2.0	1	27.1	39.1	3.9	SB(s)bc
NGC 6015	5.1 ± 0.8	2	13.6**	...	6.0	SA(s)cd
NGC 6217	19 ± 1.6	2	21.1	10.2	4.0	SB(rs)bc
NGC 6384	7.6 ± 0.7	2	24	3.27	3.6	SAB(r)bc
NGC 6503	11 ± 1.1	6	4.2	3.78	5.9	SA(s)cd
NGC 6509	5.97 ± 0.23	5	25.7*	...	6.6	SBcd
NGC 6643	14 ± 1.6	6	23.1	13.8	5.2	SA(rs)c
NGC 6814	7.5 ± 1.2	1	21.1	4.71	4.0	SAB(rs)bc
NGC 6946	394 ± 4.7	1,6	6.7	79.8	5.9	SAB(rs)cd
NGC 6951	78 ± 2.6	1,6	21.7	15.2	3.9	SAB(rs)bc
NGC 7217	7 ± 1.4	2,6	16.3	4.13	2.5	SA(r)ab
NGC 7331	19 ± 1.3	2,6	14.7	6.98	3.9	SA(s)b
NGC 7479	37 ± 2.5	1	34.7	12.9	4.4	SB(s)c
NGC 7541	49 ± 2.2	1	38.1	14.8	4.7	SB(rs)bc pec
NGC 7640	2.3 ± 0.3	2	8.5	1.33	5.3	SB(s)c
NGC 7741	1.1 ± 0.3	2,5	11.7*	...	6.0	SB(s)cd
IC 342	199 ± 3.9	1,6	3.0	65.5	5.9	SAB(rs)cd
UGC 3574	1.16 ± 0.18	5	21.9*	...	5.9	SA(s)cd
UGC 8516	1.20 ± 0.19	5	15.4*	...	5.9	Scd
MCG 1-3-85	1.39 ± 0.18	5	13.6*	...	7.0	SAB(rs)d

NOTES.—Col. (1): Galaxy name. Col. (2): Integrated intensity of ^{12}CO ($J = 1$–0) in T_{mb}. Galaxies marked with three asterisks had bad pointing accuracy. Col. (3): Reference of the CO intensity in col. (2). Col. (4): Distance to the galaxy in Mpc, from Young et al. (1995) unless otherwise noted; values marked with an asterisk are from Böker et al. (2003), values marked with two asterisks are from Braine et al. (1993), and values marked with three asterisks are from Liu & Graham (2001). Values have been converted using $H_0 = 75$ km s^{-1} Mpc^{-1}. For members of the Virgo cluster, 16.1 Mpc is assumed from Cepheid calibrations (Ferrarese et al. 1996). Col. (5): Integrated intensity $\int T_{mb}\, dv$ of the center from the FCRAO sample by Young et al. (1995) or Kenney & Young (1988) with a beam size of 45″, converted from antenna temperature T_A^* to the main beam temperature scale using a main beam efficiency of $\eta_{mb} = 0.55$ and $T_A^* = \eta_{mb} T_{mb}$. Col. (6): Hubble type, from the HyperLEDA database (Paturel et al. 2003). Col. (7): Morphology, taken from NED except for NGC 3690, which is from RC2.

REFERENCES.—(1) This study, at NRO 45 m; (2) Braine et al. 1993 at IRAM 30 m; (3) Planesas et al. 1989 at IRAM 30 m; (4) Combes et al. 1988 at IRAM 30 m; (5) Böker et al. 2003 at IRAM 30 m; (6) Nishiyama & Nakai 2001 at NRO 45 m. For galaxies outside of those observed in this study, only those detected are listed.

one beam. It is common to multiply the observed CO intensity by cos i to correct for this effect.

Figure 7 shows the variation of CO intensity on i. The observed CO intensity depends very weakly on i. If the true CO distribution within the observing beam is disklike, requiring a correction for inclination, the observed CO intensity must increase as the inclination becomes edge-on; the effective observing area of the subtended beam becomes larger, scaling as $\propto \cos i^{-1}$. This will result in a slope of -1 in the $\log I_{1\,\mathrm{kpc}}$ versus cos i figure. A least-squares fit to Figure 7 results in a slope of -0.35 ± 0.19. Although a variation of CO intensity on inclination does exist, the intrinsic dispersions in the CO intensities are far larger.

This can be explained if the effect is of geometrical quality, where i in the literature is physically not well-defined in the central regions, owing to the thickness of the disk. The molecular gas distribution in the 16″ beam may not be represented well by a disk structure, in which case a correction by a factor cos i will be artificial. This view is also supported by the fact that the trend in Figure 7 is same at different wavelengths (Komugi et al. 2007), which cannot be explained if the bias results from issues with optical depth. In the following sections, we either use the CO intensity alone (without correcting for inclination) or use intensity ratios in different beam sizes to cancel any effects from inclinations.

7. CENTRAL CONCENTRATION AND BARS

Figure 8 shows the number distribution of the ratio of molecular gas surface mass density in the central 1 kpc to the central

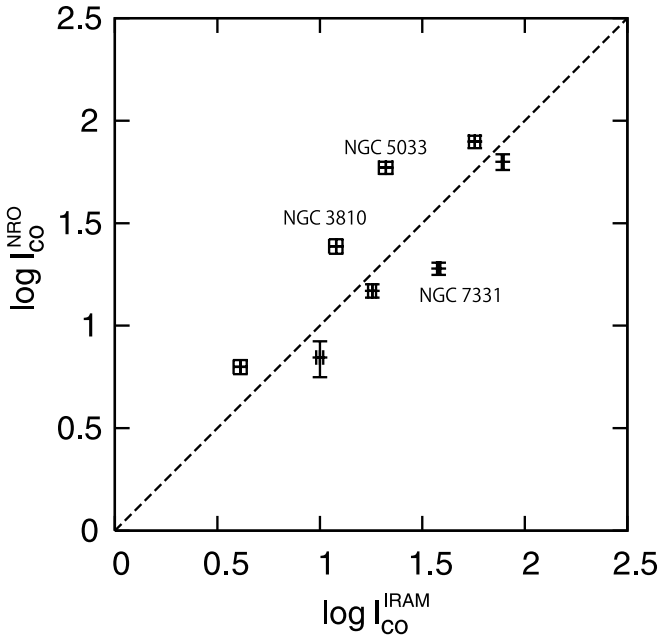

FIG. 3.—Comparison of integrated CO intensities in K km s^{-1} for galaxies that were observed with both the IRAM 30 m and NRO 45 m telescopes. The galaxies are NGC 278, NGC 628, NGC 3810, NGC 4321, NGC 4414, NGC 5033, NGC 7217, and NGC 7331. The line expresses $I_{CO}^{NRO} = I_{CO}^{IRAM}$.

3 kpc, or the central concentration, normalized to sample size. The central concentration of gas in both barred and nonbarred galaxies peak at about 1–2, but nonbarred galaxies quickly drop off above 5. Barred galaxies, however, seem to show a tail of high central molecular concentration up to 9. Above 5, barred galaxies dominate the distribution. Barred galaxies from Kuno et al. (2007) also show a higher central concentration, and Figure 8

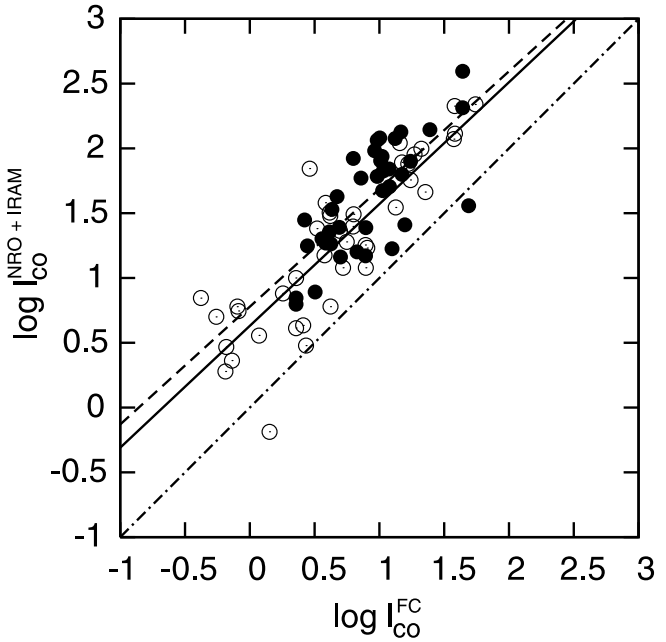

FIG. 4.—Central concentration of gas. Abscissa is integrated CO intensity from the FCRAO survey with 45″ resolution, and the ordinate is same for telescopes IRAM 30 m (*open circles*) and NRO 45 m (*filled circles*) with 22″ and 16″ resolution, respectively. The dashed line represents a least-squares fit to the NRO 45 m sample, and the solid line IRAM 30 m. The dash-dotted line represents where the ratio of abscissa and ordinate becomes unity.

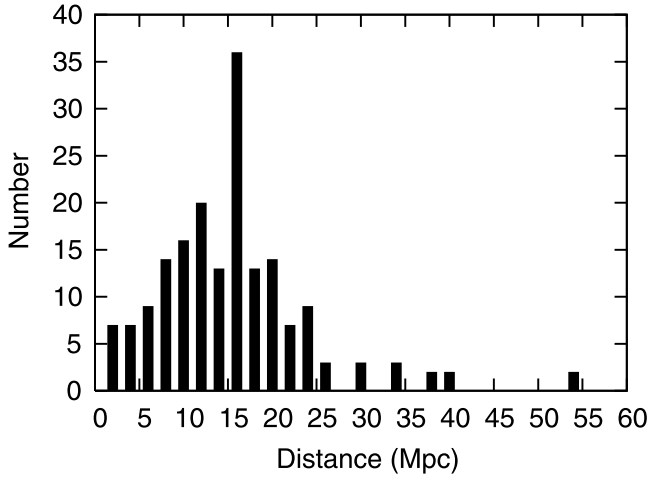

FIG. 5.—Number distribution of the distance of the sample galaxies. The strong peak at 16 Mpc are for members of the Virgo cluster.

confirms this using a large number of samples. The probability that the distribution of barred galaxies and that of nonbarred galaxies are derived from a same parent population (the Kolmogorov-Smirnov [KS] test) is $P_{KS} = 0.72$. This indicates that the barred samples cannot be said to be significantly different from nonbarred samples.

To check for any artificial effects caused by using samples at different distances (therefore probing different regions), Figure 9 shows the same figure but only for samples within the distance range of 13–19 Mpc. The trend of barred galaxies having a high central concentration tail is still seen, but with $P_{KS} = 0.76$ (see § 10 for the reason why the barred samples may not be observed to have higher central concentration as in previous studies). It is interesting that the central concentration in barred galaxies peaks at around the same value as nonbarred galaxies, but the median of the central concentration is higher for the barred galaxies. This cannot be explained by the classical picture of bars simply helping the inflow of molecular gas toward the center, because then we should expect barred galaxies to have a peak at a higher degree of central concentration.

8. CENTRAL CONCENTRATION AND HUBBLE TYPE

Figure 10 shows the CO intensity along the Hubble types, for different beam sizes. Molecular gas is significantly more massive

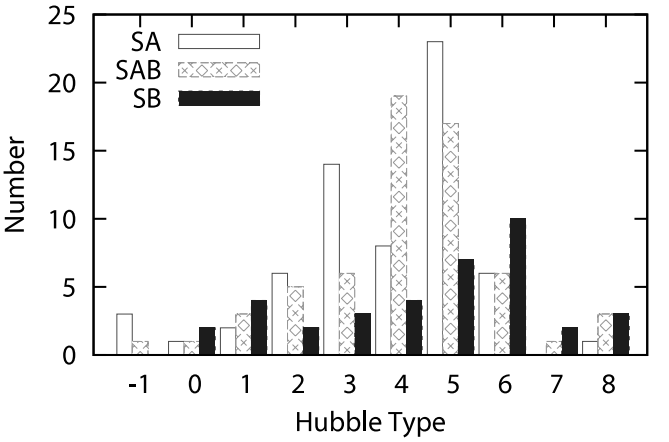

FIG. 6.—Morphological distribution of the samples in Table 2 with detected CO in the central kpc. [*See the electronic edition of the Supplement for a color version of this figure.*]

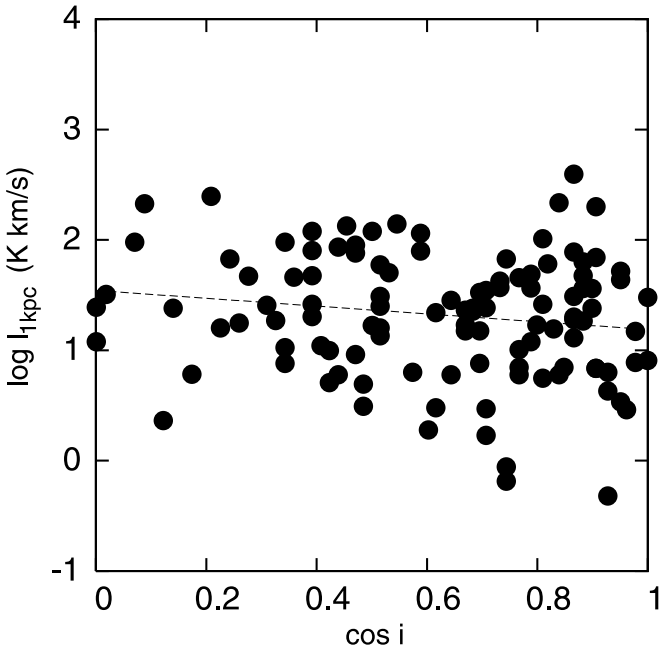

FIG. 7.—Variation of CO intensity with inclination i (0 being face-on). The line is a least-squares fit with a slope of −0.35. Galaxies that do not have normal morphology (peculiars, irregulars, and the like) have not been included.

in the central 1 kpc of early-type galaxies (*top*), where the large stellar bulge can be assumed to create a deep potential well. On the other hand, the bottom panel of Figure 10 shows CO intensity observed with the 45″ beam, or the central 3 kpc. It is apparent that molecular gas is not as well correlated with Hubble type than the central 1 kpc. The typical detection threshold in the FCRAO sample is $\sim I_{3\,\mathrm{kpc}} = 2$ K km s^{-1} (0.3 on the log scale), shown in Figure 10 by the horizontal dashed line. Many of the CO intensities in the late-type galaxies are close to this threshold, but a weak correlation with Hubble type is still observed.

This indicates that the trend in Figure 10 (*top*) is not created by the overall low molecular gas mass in the central regions of late-type galaxies, but that the gas distribution is more extended in late-type galaxies. Figure 11 shows the ratio of CO intensity

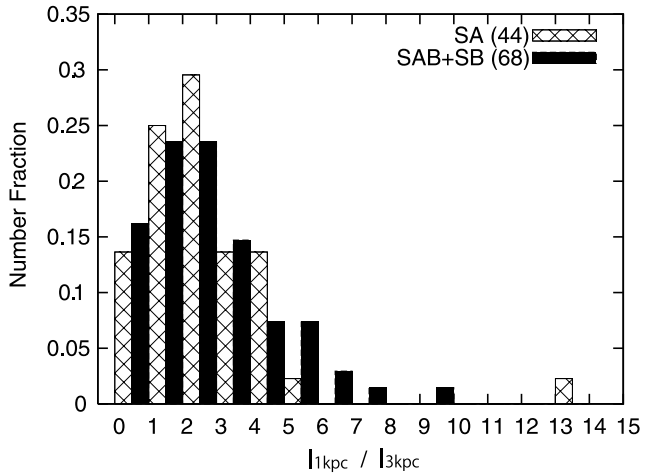

FIG. 8.—Number fraction distribution of central concentration of molecular gas for all samples with 16″ (or 22″) and 45″ data. Numbers in the parenthesis are the sample size. Note the tail of high concentration for barred galaxies. One non-barred S0 galaxy, NGC 4438, shows $I_{1\,\mathrm{kpc}}/I_{3\,\mathrm{kpc}} = 13$, which is more than the formal upper limit determined by the area of the two observing beams. This can be attributed to the uncertainties of the observations.

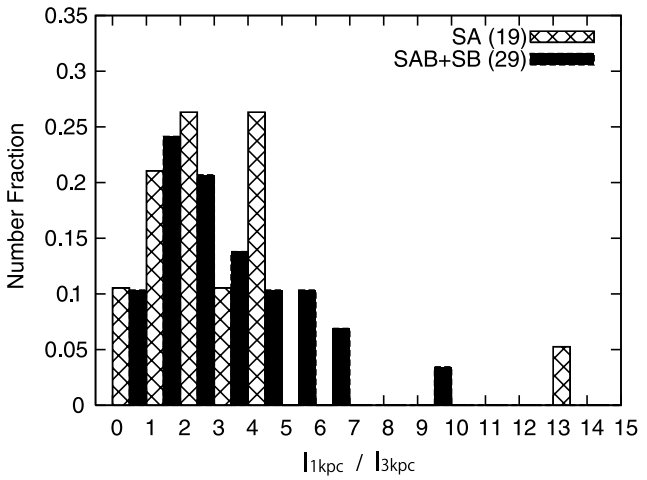

FIG. 9.—Same as Fig. 8, but for a subsample of galaxies within the distance range of 13–19 Mpc. Most are members of the Virgo cluster. Barred galaxies dominate the central concentration above 5.

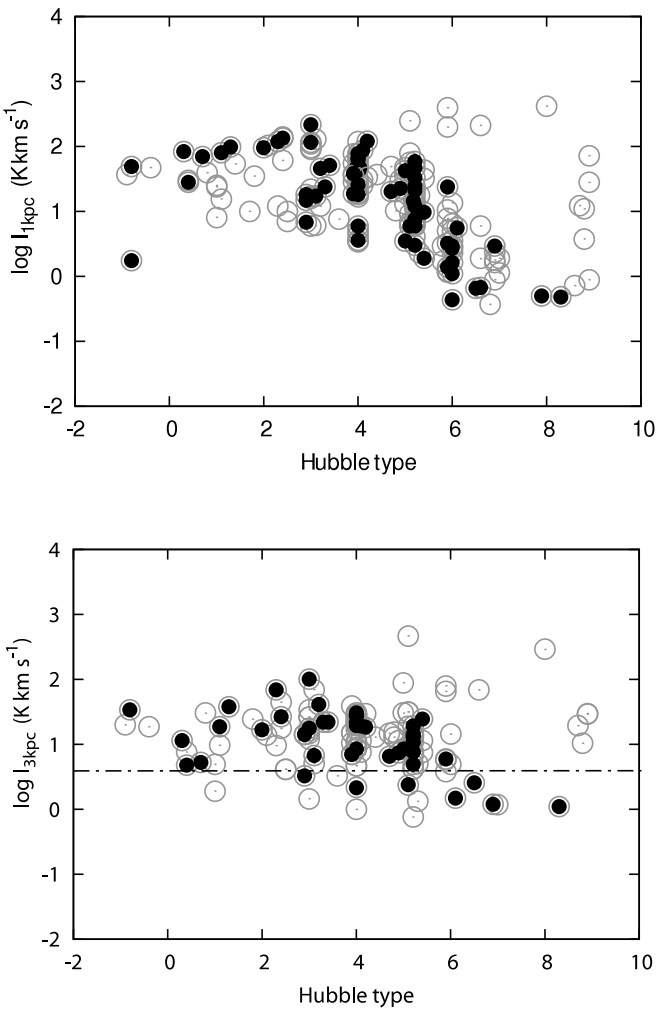

FIG. 10.—*Top*: Distribution of CO intensity in the central 1 kpc with Hubble type. Filled circles are galaxies within the distance of 13–19 Mpc and show a somewhat tighter relation, which can probably be attributed to certainty in distance. *Bottom*: Same as top figure, for a the central 3 kpc. The trend with Hubble type is not apparent here. [*See the electronic edition of the Supplement for a color version of this figure.*]

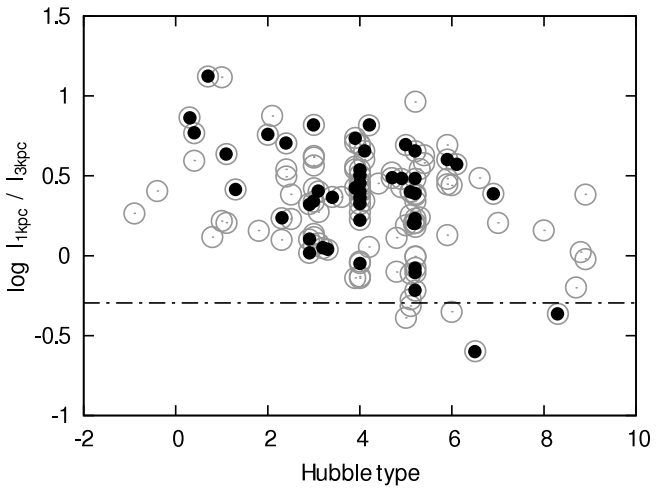

FIG. 11.—Ratio of CO intensity within the central 1 kpc and 3 kpc. Open circles represent all samples, and filled circles galaxies within the distance range 13–19 Mpc. Considering the factor of 2–3 difference in beam size (factor of 9 difference in subtending beam area), the upper limit for the ratio is 9; values above this in the figure can be attributed to errors in the measurements and should not be considered real. [*See the electronic edition of the Supplement for a color version of this figure.*]

observed with different beam sizes, and we see that the distribution of molecular gas is a smooth function of Hubble type, in that late-type galaxies have more extended gas in the center. For the earliest galaxies (Hubble type $\sim$0, corresponding to S0/S0a), the intensity ratio $\log I_{1\ \mathrm{kpc}}/I_{3\ \mathrm{kpc}}$ is close to 1, where virtually all the gas is confined to the central 1 kpc. For the latest types, however, $\log I_{1\ \mathrm{kpc}}/I_{3\ \mathrm{kpc}}$ falls to 0, indicating that there is no apparent central concentration of gas comparing the central 1 and 3 kpc, so that the molecular gas disk is likely extended beyond the central 3 kpc. The horizontal dashed line in Figure 11 is the threshold below which nondetections in the FCRAO sample increase, assuming a typical $\log I_{1\ \mathrm{kpc}} = 0$ for the latest types and $\log I_{3\ \mathrm{kpc}} = 0.3$ for the FCRAO sample. In case a bias exists in the FCRAO sample such that weak latest type galaxies are not observed, the corresponding galaxies will be plotted above this line. The absence of early-type galaxies with low central concentration, however, still points to the reality of this trend of lower central concentration toward later type galaxies.

9. ROLE OF BARS WITHIN HUBBLE TYPES

The previous sections have revealed that Hubble type can play an important role in centrally concentrating molecular gas. Bars are also known to centrally concentrate gas, although this is not found to be statistically significant based on our current data (see § 10 for possible reasons).

The main setbacks of previous studies is that they have not been able to solve the degeneracy between the effect of Hubble type and bars because of small sample size. It is of interest, therefore, which effect (bars or Hubble type) plays the dominant role in concentrating molecular gas.

Our sample enables the categorization and comparison of different Hubble types and the presence of bars, simultaneously. Figure 12 shows the CO intensity (molecular gas mass within the central 1 kpc) for early- and late-type galaxies, respectively, for barred and nonbarred galaxies. The bottom panel shows the same figure as the top and middle, but for barred and nonbarred galaxies combined. The samples were categorized into early-type (types -1 to 4.5) and late-type (types 4.5 to 9) somewhat arbitrarily, so that both samples had significant numbers of galaxies.

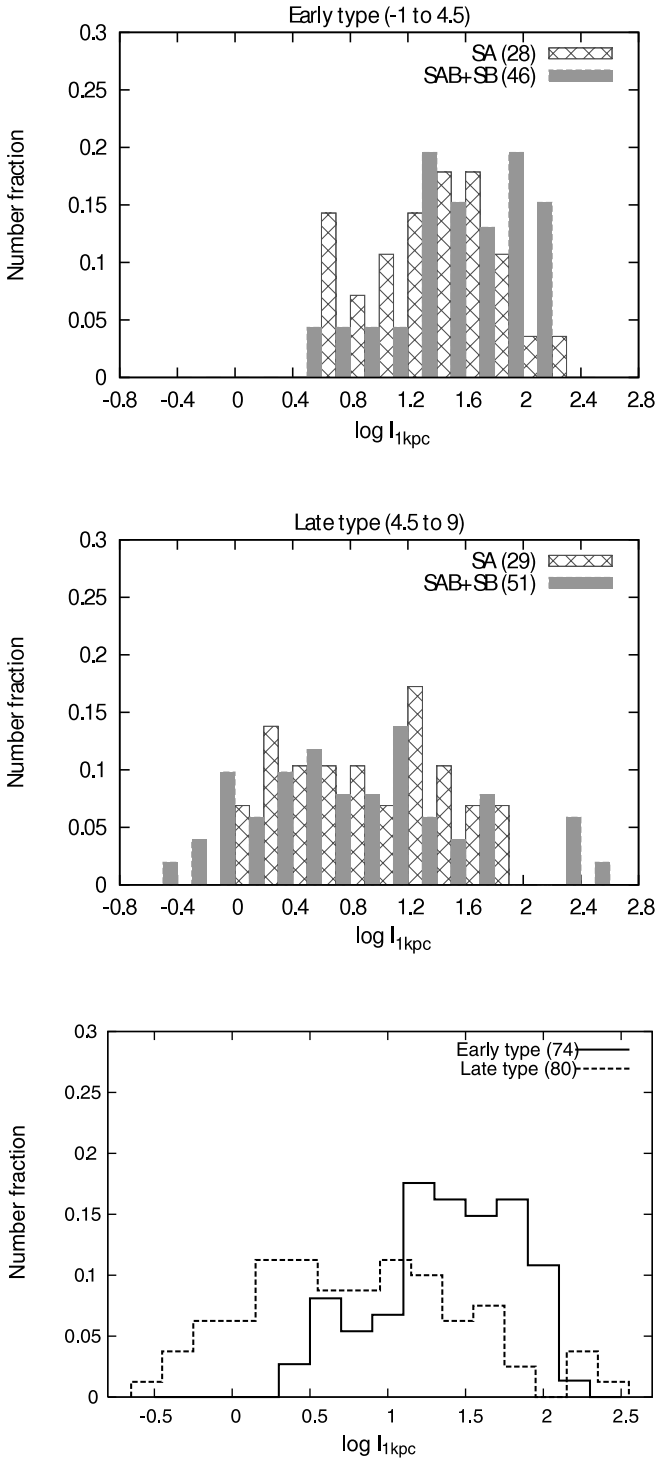

FIG. 12.—Distribution of CO intensity for the central 1 kpc for early-type (*top*) and late-type (*middle*) galaxies. The two groups have a distinctively different distribution. The bottom figure shows the histogram for the early- and late-types, without regard to the presence of bars. [*See the electronic edition of the Supplement for a color version of this figure.*]

If bars concentrate gas into the central region regardless of Hubble type, we can expect I_{CO} to be higher in barred galaxies compared with nonbarred galaxies, both in early- and late-types. In fact, Figure 11 (*top*) seems to suggest that barred early-type galaxies have a top-heavy molecular mass distribution compared with nonbarred early-types with a slightly higher mean CO intensity. This trend is not statistically significant, however, with

$P_{KS} = 0.50$. For barred and nonbarred late-type galaxies, P_{KS} is 0.31. This is not significant either, and it is clear from Figure 12 (*middle*) that the apparent difference in the two distributions results from a wider distribution of CO intensity in barred late-type galaxies. Four barred late-type galaxies have high molecular gas mass ($\log I_{CO} \geq 2.0$). All of these are known starburst galaxies (NGC 253, IC 342, NGC 3079, and NGC 6946). Except for these four, barred galaxies in late-types do not show a high gas density distribution; barred galaxies in late-types apparently do not have the high gas density expected from gas angular momentum redistribution. In cases in which the gas is concentrated, they have extremely concentrated gas and an associated starburst. This leads us to speculate that these high central concentration late-type starbursts may either be on the verge of evolving to early-type galaxies if the starburst is strong enough (in the context of secular evolution) or just using up the molecular fuel to move its place in Figure 12 (*middle*) to the least massive barred late-types, which also show a distinctive tail from nonbarred late-types.

If the presence of a bulge and its stellar potential drives molecular gas into the central region regardless of whether they have bars, we can expect early-type nonbarred galaxies to have higher $I_{1\,kpc}$ than late-type nonbarred galaxies. In fact, these two are likely to be significantly different, with $P_{KS} = 0.06$. The average CO intensity in early nonbarred galaxies ($I_{1\,kpc} = 45.1$ K km s^{-1}) is more than 2 times larger than late nonbarred galaxies ($I_{1\,kpc} = 18.9$ K km s^{-1}). The bulge potential seems very effective in concentrating molecular gas into the central 1 kpc. Barred early-type galaxies also significantly differ from barred late-types, with $P_{KS} \leq 0.001$. In the same way, with the barred and nonbarred galaxies combined, early-type galaxies and late-type galaxies are, again, significantly different ($P_{KS} \leq 0.001$). From these analyses, it seems that the bulge potential (Hubble type) is the more effective parameter in changing I_{CO} in the central 1 kpc than bars. The possibility of early-type galaxies showing more massive molecular gas in the central 1 kpc only because of stronger bars than late-types is rejected.

It is also important, however, to normalize the CO intensity in the central 1 kpc with CO data in a larger area to more accurately address the central concentration of molecular gas. Figure 13 shows the ratio of molecular mass in the central 1 kpc to the central 3 kpc for early- and late-type galaxies. The bottom figure is the same as the top and middle but with barred and nonbarred galaxies combined. The high central concentration tail (see § 8) in the distribution can be seen for early-type galaxies but not late-types (meaning that early-type galaxies constitute the high-concentration tail in Fig. 8). The KS test shows that the probability of barred galaxies and nonbarred galaxies for the early-type group derived from the same parent group is $P_{KS} = 0.62$. Molecular gas in barred early-type galaxies are not significantly more centrally concentrated than nonbarred early-types, but the tail of higher concentration in barred galaxies can still be seen, the median concentration being 1.6 times higher in barred early-types.

The central concentrations in late-type galaxies in Figure 12 (*middle*) seem much more insensitive to the presence of bars. The tail of higher concentration that was seen in early-types are not seen. The only exception of a highly centrally concentrated barred late-type galaxy is NGC 3486, with practically all of the gas within its central 1 kpc. This SABc galaxy is only weakly barred, with a bar strength (ratio of maximum tangential force and average radial force) of 0.2 (Laurikainen & Salo 2002). The central concentration of molecular gas in this galaxy is extraordinary in terms of bar and Hubble type, within the context of this paper. The KS-test for barred and nonbarred galaxies in the late-type group shows that the two morphologies can be derived from a same distribution by $P_{KS} = 0.71$ probability.

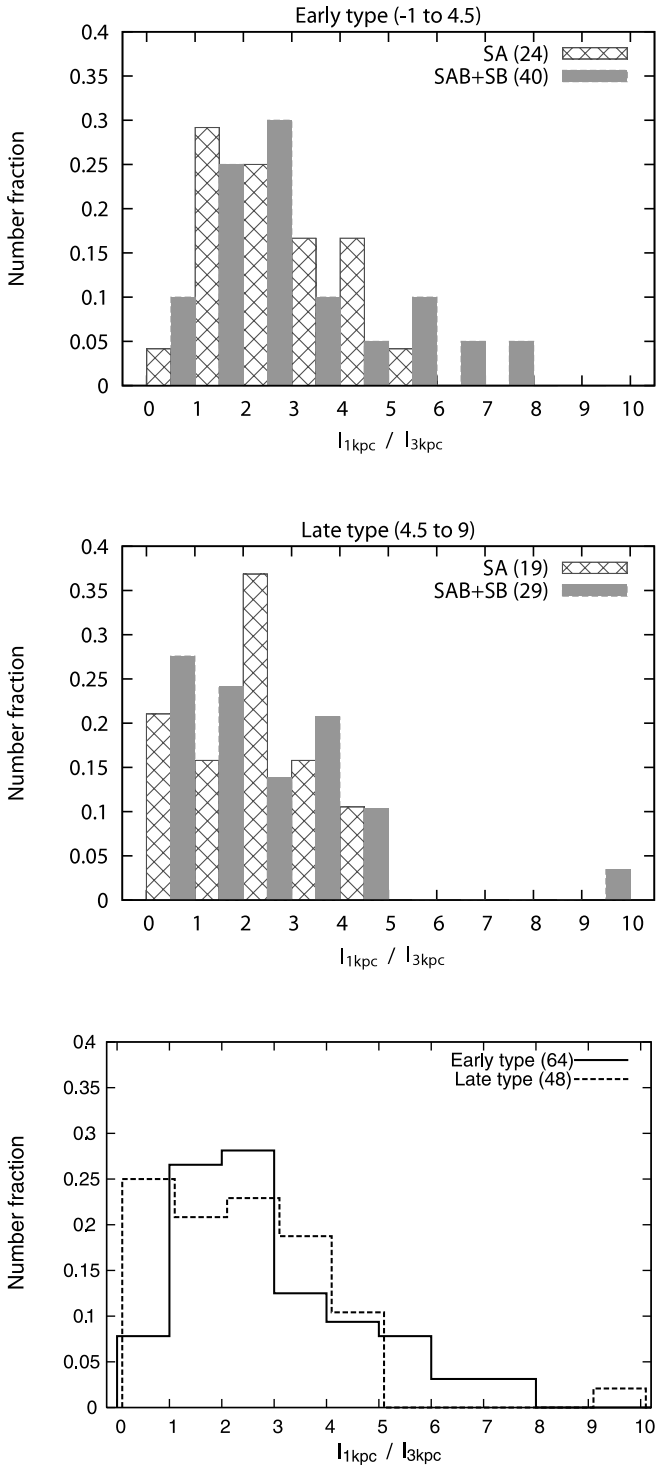

FIG. 13.—Distribution of $I_{1\,kpc}/I_{3\,kpc}$ for early-type (*top*) and late-type (*middle*) galaxies. The high central concentration tail seen in the top figure is not seen in the middle figure. The bottom figure shows the histogram for the early- and late-types, without regard to the presence of bars. [*See the electronic edition of the Supplement for a color version of this figure.*]

Comparing nonbarred early-types and nonbarred late-types give $P_{KS} = 0.26$. Similarly, barred early-types and barred late-types give $P_{KS} = 0.39$.

From the bottom panel of Figure 13, we see that almost all early-type galaxies have a ratio $I_{1\,kpc}/I_{3\,kpc}$ of more than 1, indicating

that the central 1 kpc is almost always denser than its surroundings. Late-type galaxies, on the other hand, actually peak at <1, meaning that many late-type galaxies are less dense in the central kpc compared with the surrounding disk. Early-type galaxies are more likely to be centrally concentrated than late-types ($P_{\rm KS} = 0.25$).

10. DISCUSSION

Central concentration of molecular gas from bars in early-type (Sbc and earlier) galaxies had already been found by Sheth et al. (2005), where early barred galaxies showed concentration enhancement of a factor of 4 compared with early nonbarred galaxies. The median central concentration for our sample of early-type bars ($\sim$4.1) is also higher than early-type nonbars ($\sim$2.6), although not by a factor of 2. Our definition of central concentration $I_{1\ {\rm kpc}}/I_{3\ {\rm kpc}}$ employs the molecular mass in the central 45″ for normalization, whereas the Sheth et al. (2005) sample uses the global molecular mass. Since the central 45″ ($\sim$3 kpc) would likely not contain all of the galaxy's molecular gas, any trends in the central concentration would be mitigated compared with normalizations using the whole molecular content. Kuno et al. (2007), similarly, used CO maps to define the central concentration of molecular gas in a sample of 40 galaxies. They found barred galaxies are significantly ($P_{\rm KS} = 0.004$) more centrally concentrated than nonbarred galaxies. Therefore, our result that barred galaxies are not significantly more concentrated ($P_{\rm KS} = 0.76$) is likely to be a result of using the central 45″ for normalization rather than the central concentration being not as strong. Errors in the measurements, which can change the derived CO intensity by factor of 2 when comparing different telescopes, can also reduce the power of comparison with the FCRAO measurements. These sources of error apply to the whole sample, however, and the observed result that Hubble type affects the central concentration more effectively than bars will likely not be changed.

11. SUMMARY AND CONCLUSIONS

This paper outlined a CO survey of nearby galactic centers conducted with the NRO 45 m telescope. Combined with published data at similar and lower resolution, we are able to infer on the molecular gas distribution in barred and unbarred galaxies of various Hubble types. The number of galaxies used ($\sim$160) is far more than that used in previous interferometric and single-dish mapping studies. The main results of this study are as follows:

1. Molecular gas is denser in nonbarred early-type galaxies compared with nonbarred late-type galaxies. Therefore, possible stronger bars in early-types cannot be the dominant reason for massive molecular gas observed in early-types.
2. Central concentration of molecular gas in early-type galaxies is confirmed. The ratio of molecular gas in the central kiloparsec to the central 3 kpc declines smoothly with Hubble type.
3. Barred early-type galaxies have a higher median of central concentration than nonbarred early-type galaxies, suggesting a tail distribution of high central concentration in barred galaxies, although not statistically significant based on the current data. This trend is not observed in late-type galaxies.

The authors thank the anonymous referee for valuable comments and careful reading of the manuscript. The authors also wish to thank the NRO staff for generous allocation of telescope time. S. K., S. O., F. E., and K. M. were financially supported by a Research Fellowship from the Japan Society for the Promotion of Science for Young Scientists. We acknowledge the usage of the HyperLeda database (http://leda.univ-lyon1.fr), and the NASA/IPAC Extragalactic Database (NED), which is operated by the Jet Propulsion Laboratory, Caltech, under contract with the National Aeronautics and Space Administration.

REFERENCES

Abraham, R. G., & Merrifield, M. R. 2000, AJ, 120, 2835
Athanassoula, E. 1992, MNRAS, 259, 34
Böker, T., Lisenfeld, U., & Schinnerer, E. 2003, A&A, 406, 87
Braine, J., Combes, F., Casoli, F., Dupraz, C., Gerin, M., Klein, U., Wielebinski, R., & Brouillet, N. 1993, A&AS, 97, 887
Combes, F., Dupraz, C., Casoli, F., & Pagani, L. 1988, A&A, 203, L9
Combes, F., & Gerin, M. 1985, A&A, 150, 327
Dressel, L. L., & Condon, J. J. 1976, ApJS, 31, 187
Ferrarese, L., et al. 1996, ApJ, 464, 568
Helfer, T. T., Thornley, M. D., Regan, M. W., Wong, T., Sheth, K., Vogel, S. N., Blitz, L., & Bock, D. C.-J. 2003, ApJS, 145, 259
Ho, L. C., Filippenko, A. V., & Sargent, W. L. W. 1997, ApJS, 112, 315
Kenney, J. D., & Young, J. S. 1988, ApJS, 66, 261
Komugi, S., Kohno, K., Tosaki, T., Nakanishi, H., Onodera, S., Egusa, F., & Sofue, Y. 2007, PASJ, 59, 55
Kuno, N., et al. 2007, PASJ, 59, 117
Laurikainen, E., & Salo, H. 2002, MNRAS, 337, 1118
Laurikainen, E., Salo, H., Buta, R., & Vasylyev, S. 2004, MNRAS, 355, 1251
Liu, M. C., & Graham, J. R. 2001, ApJ, 557, L31
Nishiyama, K., & Nakai, N. 2001, PASJ, 53, 713
Paturel, G., Petit, C., Prugniel, P., Theureau, G., Rousseau, J., Brouty, M., Dubois, P., & Cambrésy, L. 2003, A&A, 412, 45
Pfenniger, D., & Norman, C. 1990, ApJ, 363, 391
Planesas, P., Gomez-Gonzalez, J., & Martin-Pintado, J. 1989, A&A, 216, 1
Sakamoto, K., Okumura, S. K., Ishizuki, S., & Scoville, N. Z. 1999a, ApJS, 124, 403
———. 1999b, ApJ, 525, 691
Sheth, K., Vogel, S. N., Regan, M. W., Thornley, M. D., & Teuben, P. J. 2005, ApJ, 632, 217
Sofue, Y., Koda, J., Nakanishi, H., Onodera, S., Kohno, K., Tomita, A., & Okumura, S. K. 2003a, PASJ, 55, 1189
Wada, K., & Habe, A. 1995, MNRAS, 277, 433
Young, J. S., Allen, L., Kenney, J. D. P., Lesser, A., & Rownd, B. 1996, AJ, 112, 1903
Young, J. S., & Knezek, P. M. 1989, ApJ, 347, L55
Young, J. S., et al. 1995, ApJS, 98, 219